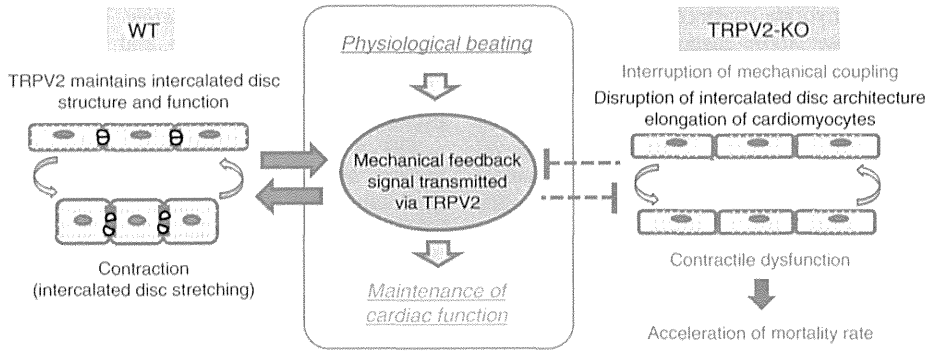

Figure 10 | Role of TRPV2 within the working heart. In wild-type mice, TRPV2 protein (yellow) is located in the intercalated discs (red), which is cyclically stretched and accompanied by cardiac contractions within the working heart. The mechanical feedback signal transmitted via TRPV2 is crucial for the maintenance of cardiomyocytes. TRPV2 ablation leads to the disruption of the intercalated disc architecture (red), and disorganization of sarcomere myofibril proteins at the intercalated discs (orange). These TRPV2-KO myocytes show contractile dysfunction. Therefore, the mortality rate of TRPV2-KO mice is accelerated. Thus, the mechanical feedback signal within the working heart integrates myocyte structure and function, with TRPV2 playing a pivotal role.

involved in myocyte E–C coupling and the mechanical signal mediated by TRPV2 are spatially and temporally controlled by different signals in cardiomyocytes. Further studies might clarify the molecular mechanism of mechanotransduction mediated by TRPV2 in cardiomyocytes, and so improve our understanding of cardiac development and maturation, hypertrophic remodelling in the heart and the pathophysiology of heart disease.

Recently, Rubinstein *et al.*[38] reported the cardiac function of TRPV2-KO mice expressing *Cre* under the control of the cytomegalovirus promoter generated by Park *et al*[39]. They observed that cardiac function declined in TRPV2-deficient mice compared with controls, despite no histological abnormality[38]. Although there are differences in the severity of cardiac dysfunction and the depression of myocyte contractility, these results are consistent with our observations. However, the construction of their TRPV2-KO mice differed from our model in the site at which the partial elimination occurred, which corresponded to the channel pore and carboxy-terminal region of TRPV2, using a ubiquitous promoter, and the genetic background of the mice (B6129SF2/J)[39]. Park *et al.*[39] have reported that their model was susceptible to perinatal lethality but displayed normal thermal and mechanical nociception. They therefore suggested the possibility that compensatory mechanisms prevented the obvious phenotype of TRPV2-deficient cells being reflected in their KO mice[39]. On the other hand, the cardiac-specific elimination of TRPV2 in this study affected neither the embryonic development nor the growth after birth, in the absence of tamoxifen administration. Taken together, we believe that the acute elimination of TRPV2 function in our model might circumvent any hypothetical compensatory process.

Methods

Animals. Mice were housed under a 12-h light–dark cycle in a temperature-controlled environment. All the experiments were performed in male mice aged 10 weeks old (weighing 22–24 g). Littermates were used in this study to randomize genetic variation. All animal experiments were approved by the Animal Research Committee of Okayama University (Okayama, Japan), and were performed in accordance with institutional guidelines.

Generation of TRPV2 conditional KO mice. All experiments requiring gene recombination in this study were carried out in accordance with the institutional guideline of Okayama University (Okayama, Japan). Using cloned TRPV2 cDNA (accession code. NM011706) as a probe, we screened a genomic library constructed from C57/BL6J mouse DNA. The genomic clone was used to generate the targeting vector shown in Supplementary Fig. 1, which was linearized for electroporation into C57/BL6J ES cells. After selection, G418-resistant ES clones were screened for the presence of the targeted locus by southern blot analysis. Targeted ES cells were microinjected into Balb/c mouse blastocysts, and germline transmission of the TRPV2 conditional null alleles was confirmed by southern blotting and PCR genotyping using genomic DNA extracted from mouse tail veins. We crossed mice carrying a $TRPV2^{flox}$ allele with transgenic mice (*MerCreMer*) expressing tamoxifen-inducible cardiomyocyte-specific Cre recombinase to produce $TRPV2^{flox/flox}$;$MerCreMer^{+/-}$ mice. Germline transmission of TRPV2 conditional null alleles was confirmed by southern blotting and PCR genotyping using the primer pair 5′-TTAAATGACTTGTGAGGGAGATAGC-3′ and 5′-CAAGTAACA CAATCTACCCAAGGTC-3′, yielding 322 (wild-type) and 369 (null allele) bp products. To induce *Cre*-mediated recombination, we injected 10-week-old male $TRPV2^{flox/flox}$;$MerCreMer^{+/-}$, $TRPV2^{flox/+}$;$MerCreMer^{+/-}$ and $TRPV2^{flox/flox}$;$MerCreMer^{-/-}$ mice intraperitoneally with 8 mg kg^{-1} tamoxifen (Sigma) once daily for 4 consecutive days. Tamoxifen injection and subsequent analyses were performed in a blinded fashion.

Electrocardiography. Transthoracic electrocardiography (ECG) was used to evaluate cardiac function with the Aplio 300 (Toshiba Medical System) and a 14-MHz transducer. The 10-week-old male mice were anesthetized initially with 2% isoflurane, and then at 1% during the examination. Left ventricular short-axis dimensions at the tip of the papillary muscles were measured on M-mode. Fractional shortening was calculated as (LVDd–LVDs)/LVDd × 100 (%).

Blood pressure measurement. Chronic measurements of blood pressure and ECG were performed on unrestrained, conscious mice (10-week-old, male) using a commercially available telemetry and computer-based data acquisition system (Data Sciences International) according to the manufacturer's instructions. Briefly, a pressure-sensing catheter was implanted in the thoracic aorta via the left carotid artery, and two electrodes were placed subcutaneously on the right shoulder and left inguinal region to record lead II ECG under anaesthesia with 2% isoflurane inhalation. Mice were returned to their home cage (placed on top of telemetry receivers), and blood pressure and ECG were continuously monitored and recorded.

Administration of IGF-1. Recombinant human IGF-1 was purchased from Cell Science, and diluted with 0.9% NaCl at a concentration of 10 mg ml^{-1} and administered to mice (60 μg per day) by continuous infusion (0.25 μl h^{-1}) using a mini osmotic pump (Alzert 1002). IGF-1 administration and tamoxifen treatment were started at the same time. Control mice received vehicle alone.

Neonatal cardiomyocyte culture. Primary cardiomyocyte cultures were prepared from ventricles of 1-day-old mice by very gentle trypsinization at room temperature, by a modification of preparation methods from rat neonatal heats[40]. Hearts were rapidly removed from neonatal $TRPV2^{flox/flox}$;$MerCreMer^{+/-}$ or $TRPV2^{flox/flox}$;$MerCreMer^{-/-}$ mice anesthetized with an overdose of diethyl ether. The ventricles were excised, cut into several pieces and washed three times with 10 ml ice-cold phosphate-buffered saline for 1 min by gentle shaking. The tissue pieces were digested three times with 0.06% trypsin in DMEM (8 ml) for 8 min at 37 °C by gentle agitation. The cell suspension was resuspended in DMEM with 10% fetal calf

serum (FCS) to stop trypsinization, and was centrifuged at 14*g* for 3 min. The cell pellets were resuspended in fresh DMEM containing 10% FCS, and plated on collagen-coated 24-well dishes at a density of 4×10^4 cells per well and maintained in DMEM containing 10% FCS. The formation of myocytes clusters and the spontaneous synchronized beating were confirmed by inverted microscope (CKX41, Olympus).

Stretch stimulation of cardiomyocytes. For stretch stimulation of cardiomyocytes, the cell suspension were plated on 1 cm^2 collagen-coated polydimethylsiloxane stretch chambers at 2×10^5 cells per well, and cultured. After 24 h, primary cardiomyocytes were divided into two groups and maintained for up to 2 days in DMEM containing 10% FCS, with or without tamoxifen (0.2 μM ml^{-1}). Membranes were uniformly stretched by 20% for 3 s, using a computer-controlled stepping motor machine (STB-150, STREX), by a slight modification of cell-stretch culture methods[41]. One end of the chamber was firmly attached to a fixed frame, while the other was attached to a movable frame connected to a motor-driven shaft. The amplitude and frequency of stretch were controlled by a programmable microcomputer. The silicon membrane was uniformly stretched over the whole membrane area, and the lateral thinning did not exceed 1% at 20% stretch. TRPV2 deficiency did not have a discernible impact on the cardiomyocytes' ability to adhere to the membrane, although the cell–cell interfaces with neighbouring myocytes were expanded.

Stretch-induced Ca^{2+}-transients in newborn cardiomyocytes. Stretch-induced Ca^{2+} transients were examined in cardiomyocytes loaded with 2 μM fura-2 acetoxymethyl ester (fura-2) for 30 min at 37 °C and maintained in standard Tyrode's solution under continuous flow using a microperfusion system. Fura-2-loaded cells were alternately excited at 340 and 380 nm using a Lambda DG-4 Ultra High Speed Wavelength Switcher (Sutter Instruments) coupled to an inverted IX71 microscope with a UApo 20 × /0.75 objective lens (Olympus). Fura-2 fluorescent signals were recorded (ORCA-Flash 2.8; Hamamatsu Photonics) and analysed by a ratiometric fluorescence method using MetaFluor software (version 7.7.5.0; Molecular Devices).

Isolation of adult mouse ventricular myocytes. Ventricular myocytes were obtained from 10-week-old male *TRPV2$^{flox/flox}$;MerCreMer$^{+/-}$* and *TRPV2$^{flox/flox}$;MerCreMer$^{-/-}$* mice by a slight modification of Shioya's methods[42]. Hearts were rapidly removed from adult *TRPV2$^{flox/flox}$;MerCreMer$^{+/-}$* or *TRPV2$^{flox/flox}$;MerCreMer$^{-/-}$* mice anesthetized with an overdose of pentobarbital (300 mg kg^{-1}, intraperitoneally), and Langendorff perfused at a constant hydrostatic pressure of 70 cm H_2O at 37 °C using cell isolation buffer (CIB) supplemented with 0.4 mM EGTA (EGTA–CIB), which chelates calcium within the heart. CIB contained 130 mM NaCl, 5.4 mM KCl, 0.5 mM $MgCl_2$, 0.33 mM NaH_2PO_4, 22 mM glucose, 50 nM ml^{-1} bovine insulin (Sigma) and 25 HEPES-NaOH (pH = 7.4). Insulin was used from 1 U ml^{-1} stock solution in 0.1 mM HCl (pH = 4.0). EGTA was from 400 mM stock in 1 M NaOH (pH = 7.8). The perfusate was then switched to the enzyme solution (15 ml), which was CIB supplemented with 0.3 mM $CaCl_2$, 1 mg ml^{-1} collagenase (Worthington Biochemical), 0.06 mg ml^{-1} trypsin (Sigma) and 0.06 mg ml^{-1} protease (Sigma). Once the tissue had undergone complete digestion, the ventricles were excised, cut into several pieces and further digested in fresh enzyme solution (15 ml) for 15–20 min at 37 °C until they were mostly dissociated. In this enzyme solution, the $CaCl_2$ level was increased to 0.7 mM, and 2 mg ml^{-1} BSA (Sigma) was supplemented. The cell suspension was centrifuged at 14*g* for 3 min. The cell pellet (~0.1 ml) was resuspended in CIB supplemented with 1.2 mM $CaCl_2$ and 2 mg ml^{-1} BSA, and then incubated at 37 °C for 10 min, centrifuged (14*g*, 3 min) and resuspended in 10 ml Tyroad solution supplemented with 2 mg ml^{-1} BSA. Tyrode's solution contained 140 mM NaCl, 5.4 mM KCl, 1.8 mM $CaCl_2$, 0.5 mM $MgCl_2$, 0.33 mM NaH_2PO_4, 11 mM glucose and 5 mM HEPES-NaOH (pH = 7.4)[40,42].

Cell shortening and Ca^{2+} transients in adult cardiomyocytes. Isolated cardiomyocytes were loaded with 10 μmol l^{-1} Indo-1 AM (Invitrogen) and electrically stimulated at 1 Hz using a two-platinum electrode insert connected to a bipolar stimulator (Nihon Kohden, SEN-3301) on the stage of an inverted microscope (IX71, Olympus) with a × 20 water immersion objective lens (UApo N340, Olympus). Calcium transients were measured as the ratio of fluorescence emitted at 405/480 nm after excitation at 340 nm using a high-performance Evolve EMCCD camera (Photometrics). Cardiomyocytes were maintained under continuous flow in standard Tyrode's solution, exchanged using a microperfusion system. For measuring caffeine-induced calcium transients, cells were paced at 1 Hz prior to induction of caffeine contractures. Electrical stimulation was stopped 15 s before rapid perfusion with a 10 mmol l^{-1} caffeine solution. The experiments were recorded and analysed using MetaMorph software (version 7.7.1.0; Molecular Devices). Results were the means of the fluorescent signals from 10–20 cardiomyocytes from a single heart.

Measure of IGF-1 concentration. IGF-1 concentrations were measured in conditioned media from stretched and unstretched myocytes in a sandwich ELISA using mouse standards, according to the manufacturer's guidelines (R&D Systems), which quotes the sensitivity of this assay as 30 ng ml^{-1}. Standard curves and positive controls were included in each assay, and IGF-1 concentrations were obtained by interpolation.

Real-time PCR. The Mouse PI3K-AKT Signalling Pathway RT^2 Profiler PCR Array was purchased from Qiagen. Total RNA extracted from *TRPV2$^{flox/flox}$;MerCreMer$^{+/-}$* or *TRPV2$^{flox/flox}$;MerCreMer$^{-/-}$* hearts with or without tamoxifen were reverse transcribed into cDNA with oligo (dT) primers using Superpscript III. Real-time PCR was performed with Step-One plus^{TM} (Applied Biosystem). Statistical analysis of the results was performed with the $^{\Delta}$Ct value ($Ct_{\text{gene of interest}} - Ct_{\beta\text{-actin}}$). Relative gene expression was obtained using the $^{\Delta\Delta}$Ct method ($Ct_{\text{sample}} - Ct_{\text{calibrator}}$) using the *TRPV2$^{flox/flox}$;MerCreMer$^{-/-}$* hearts without tamoxifen as a calibrator.

Histology. Hearts were excised and immediately fixed in buffered 4% paraformaldehyde, embedded in paraffin and sectioned to a thickness of 4 μm. We stained serial sections of samples with Masson's trichrome to evaluate gross morphology and fibrosis. The preparations were examined under a light microscope (SZX7 or BX43, Olympus).

Electron microscopy. For electron microscopy, excised hearts were fixed in 2% paraformaldehyde/2% glutaraldehyde in 0.1 M phosphate buffer, postfixed with 2% OsO4 in 0.1 M phosphate buffer and stained with uranyl acetate and lead citrate. The microtome sections were examined under a JEM-1200 electron microscope (Nihondensi Co., Japan).

Antibodies. The following antibodies were used for immunostaining or immunoblot analysis: anti-TRPV2 (1:200 dilution, AB5398, Millipore); anti-vinculin (1:100 dilution, V9131, Sigma); anti-connexin 43 (1:100 dilution, C6219, Sigma); anti-N-cadherin (1:100 dilution, 3B9, life technologies); anti-Cav3 (1:1,000 dilution, 610420, BD Pharmingen,); anti-LTCC (1:1,000 dilution, ACC033, Alomone); anti-SERCA (1:1,000 dilution, MA3919, Thermo); and anti-RyR (1:1,000 dilution, MA3916, Thermo). The anti-NCX antibody was generated in our laboratory (1:1,000 dilution).

Immunocytochemistry. For immunocytochemistry, 5 μm frozen heart sections embedded in OCT compound (Tissue-Tek) were permeabilized with 0.1% Triton X-100 and incubated with primary antibodies. For immunostaining of rat cardiomyocytes, cells immobilized on collagen-coated glass slides were fixed with 4% paraformaldehyde for 15 min at room temperature, permeabilized with 0.1% Triton X-100 and then stained with primary antibodies.These samples were then treated with Alexa Flour 488-conjugated anti-rabbit IgG (A11008, Life Technologies) or Alexa Flour 488-conjugated anti-mouse IgG (A11001, Life Technologies). Cells or secrions were examined using a confocal microscope (Fluoview FV1000, Olympus) mounted on an Olympus IX81 epifluorescence microscope with a UPlanSApo × 60/1.35 oil immersion objective lens (Olympus).

Immunoblotting. Mice hearts and kidneys were homogenized in a Hiscotron homogenizer (NITI-ON) in lysis buffer containing 20 mM HEPES (pH 7.4), 150 mM NaCl, 1% sodium deoxycholate, 1% SDS, 2 μg ml^{-1} leupeptin, 1 μg ml^{-1} aprotinin, 200 μM phenylmethylsulfonyl fluoride, and 200 μM benzamidine hydrochloride. The lysates were centrifuged at 100,000 *g* for 20 min and the supernatants were used for immunoblot analysis. Immunoreactive bands were visualized using a chemiluminescence detection system (Perkin Elmer) and an LAS3000 Luminescent Image Analyzer (Fuji Film).

Data analysis. Data were analysed by individuals who were blinded to the genotype, drug treatment or operation. Data presented here were reproducible in at least three independent experiments. Results are shown as the mean ± s.e.m. Paired data were evaluated using a Student's *t*-test. Two-way analysis of variance with Bonferroni's *post hoc* test was used for multiple comparisons wherever appropriate. The Kaplan–Meier method with a log-rank test was used for survival analysis. $P < 0.05$ was considered statistically significant.

References

1. Engler, A. J., Sen, S., Sweeney, H. L. & Discher, D. E. Matrix elasticity directs stem cell lineage specification. *Cell* **126,** 677–689 (2006).
2. McCain, M. L. & Parker, K. K. Mechanotransduction: the role of mechanical stress, myocyte shape, and cytoskeletal architecture on cardiac function. *Eur. J. Physiol.* **462,** 89–104 (2011).
3. Hill, J. A. & Olson, E. N. Cardiac plasticity. *New Engl. J. Med.* **358,** 1370–1380 (2008).
4. Estigoy, C. B. *et al.* Intercalated discs: multiple proteins perform multiple functions in non-failing and failing human hearts. *Biophys. Rev.* **1,** 43–49 (2009).
5. Noorman, M. *et al.* Cardiac cell-cell junctions in health and disease: electrical versus mechanical coupling. *J. Mol. Cell. Cardiol.* **47,** 23–31 (2009).

6. McCain, M. L. *et al.* Cooperative coupling of cell-matrix and cell-cell adhesions in cardiac muscle. *Proc. Natl Acad. Sci. USA* **109,** 9881–9886 (2012).
7. Perriard, J.-C., Hirschy, A. & Ehler, E. Dilated cardiomyopathy: a disease of the intercalated disc? *Trends Cardiovasc. Med.* **13,** 30–35 (2003).
8. Kostetskii, I. *et al.* Induced deletion of the N-cadherin gene in the heart leads to dissolution of the intercalated disc structure. *Circ. Res.* **96,** 346–354 (2005).
9. Parlakian, A. *et al.* Temporally controlled onset of dilated cardiomyopathy through disruption of the SRF gene in adult heart. *Circulation* **112,** 2930–2939 (2005).
10. Li, J. *et al.* Loss of alphaT-catenin alters the hybrid adhering junctions in the heart and leads to dilated cardiomyopathy and ventricular arrhythmia following acute ischemia. *J. Cell Sci.* **125,** 1058–1067 (2012).
11. Wang, X. & Gerdes, A. M. Chronic pressure-overload cardiac hypertrophy and failure in guinea pigs: III. Intercalated disc remodeling. *J. Mol. Cell. Cardiol.* **31,** 333–343 (1999).
12. Alcalai, R., Metzger, S., Rosenheck, S., Meiner, V. & Chajek-Shaul, T. A recessive mutation in desmoplakin causes arrhythmogenic right ventricular dysplasia, skin disorder, and woolly hair. *J. Am. Coll. Cardiol.* **42,** 319–327 (2003).
13. Protonotarios, N. & Tsatsopoulou, A. Naxos disease and Carvajal syndrome: cardiocutaneous disorders that highlight the pathogenesis and broaden the spectrum of arrhythmogenic right ventricular cardiomyopathy. *Cardiovasc. Pathol.* **13,** 185–194 (2004).
14. Basso, C. *et al.* Ultrastructural evidence of intercalated disc remodeling in arrhythmogenic right ventricular cardiomyopathy: an electron microscopy investigation on endomyocardial biopsies. *Eur. Heart. J.* **27,** 1847–1854 (2006).
15. Balse, E. *et al.* Dynamic of ion channel expression at the plasma membrane of cardiomyocytes. *Physiol. Rev.* **92,** 1317–1358 (2012).
16. Sharif-Naeini, A. *et al.* TRP channels and mechanosensory transduction: insights into the arterial myogenic response. *Eur. J. Physiol.* **456,** 529–540 (2008).
17. Iwata, Y. *et al.* A novel mechanism of myocyte degeneration involving the Ca^{2+}-permeable growth factor-regulated channel. *J. Cell Biol.* **161,** 957–967 (2003).
18. Muraki, K. *et al.* TRPV2 is a component of osmotically sensitive cation channels in murine aortic myocytes. *Cir. Res.* **93,** 829–838 (2003).
19. Sohal, D. S. *et al.* Temporally regulated and tissue-specific gene manipulations in the adult and embryonic heart using a tamoxifen-inducible Cre protein. *Cir. Res.* **89,** 20–25 (2001).
20. Hall, M. E., Smith, G., Hall, J. E. & Stec, D. E. Systolic dysfunction in cardiac-specific ligand-inducible MerCreMer transgenic mice. *Am. J. Physiol. Heart Cir. Physiol.* **301,** H253–H260 (2011).
21. Bito, V., Heinzel, F. R., Biesmans, L., Antoons, G. & Sipid, K. R. Crosstalk between L-type Ca^{2+} channels and sarcoplasmic reticulum: alterations during cardiac remodeling. *Cardiovasc. Res.* **77,** 315–324 (2008).
22. Verdonck, F., Mubagwa, K. & Sipid, K. R. $[Na^+]$ in the subsarcolemmal 'fuzzy' space and modulation of $[Ca^{2+}]_i$ and contraction in cardiac myocytes. *Cell Calcium* **35,** 603–612 (2004).
23. Atherton, B. T., Meyer, D. M. & Simpson, D. G. Assembly and remodelling of myofibrils and intercalated discs in cultured neonatal rat heart cells. *J. Cell. Sci.* **86,** 233–248 (1986).
24. Bridget, T. J., Yipi, S., Philip, A. G., Fredrick, S. & Timothy, M. G. Ca^{2+} influx through mechanosensitive Ca^{2+} channels inhibits neurite outgrowth in opposition to other influx pathways and release from intracellular stores. *J. Neurosci.* **26,** 5656–5664 (2006).
25. Bianca, C. B., Kate, L. W., Lynette, P. & Julie, R. M. Molecular distinction between physiological and pathological cardiac hypertrophy: experimental findings and therapeutic strategies. *Phamacol. Therapeutics* **128,** 191–227 (2010).
26. Takeda, N. *et al.* Cardiac fibroblasts are essential for the adaptive response of the murine heart to pressure overload. *J. Clin. Invest.* **120,** 254–265 (2010).
27. Guo, D. *et al.* Loss of PI3Kγ enhances cAMP-dependent MMP remodeling of the myocardial N-cadherin adhesion complexes and extracellular matrix in response to early biomechanical stress novelty and significance. *Cir. Res.* **107,** 1275–1289 (2010).
28. Kontoleon, P. E. *et al.* Hormonal profile in patients with congestive heart failure. *Int. J. Cardiol.* **87,** 179–183 (2003).
29. Janssen, D. A. W. *et al.* The mechanoreceptor TRPV4 is localized in adherens junctions of the human bladder urothelium: a morphological study. *J. Urol.* **186,** 1121–1127 (2011).
30. Montell, C. TRP channels in *Drosophila* photoreceptor cells. *J. Physiol.* **567,** 45–51 (2005).
31. Cao, P., Maximov, A. & Sudhof, T. C. Activity-dependent IGF-1 exocytosis is controlled by the Ca^{2+}-sensor synaptotagmin-10. *Cell* **145,** 300–311 (2011).
32. Christensen, A. P. & Corey, D. P. TRP channels in mechanotransduction: direct or indirect activation? *Nat. Rev. Neurosci.* **8,** 510–521 (2007).
33. Mercado, J., Gordon-Shaag, A., Zagotta, W. N. & Gordon, S. E. Ca^{2+}-dependent desensitization of TRPV2 channels is mediated by hydrolysis of phosphatidylinositol 4,5-phosphate. *J. Neurosci.* **30,** 13338–13347 (2010).
34. Spassova, M. A., Hewavitharana, T., Xu, W., Soboloff, J. & Gill, D. L. A common mechanism underlies stretch activation and receptor activation of TRPC6 channels. *Proc. Natl Acad. Sci. USA* **103,** 16586–16591 (2006).
35. Chemin, J. *et al.* A phospholipid sensor controls mechanogating of the K+ channel TREK-1. *EMBO J.* **24,** 44–53 (2005).
36. Kanzaki, M. *et al.* Translocation of a calcium-permeable cation channel induced by insulin-like growth factor-I. *Nat. Cell Biol.* **1,** 165–170 (1999).
37. Penna, A. *et al.* PI3-kinase promotes TRPV2 activity independently of channel translocation to plasma membrane. *Cell Calcium* **39,** 495–507 (2006).
38. Rubinstein, J. *et al.* Novel role of transient receptor potential vanilloid 2 in the regulation of cardiac performance. *Am. J. Physiol. Heart Circ. Physiol.* **306,** H574–H584 (2014).
39. Park, U. *et al.* TRP vanilloid 2 knock-out mice are susceptible to perinatal lethality but display normal thermal and mechanical nociception. *J. Neurosci.* **31,** 11425–11436 (2011).
40. Katanosaka, Y. *et al.* Calcineurin inhibits Na^+/Ca^{2+} exchange in phenylephrine-treated hypertrophic cardiomyocytes. *J. Biol. Chem.* **280,** 5764–5772 (2005).
41. Katanosaka, Y. *et al.* Analysis of cyclic stretch responses using cell-adhesion-patterned cells. *J. Biotechnol.* **133,** 82–89 (2008).
42. Shioya, T. A simple technique for isolating healthy heart cells from mouse models. *J. Physiol. Sci.* **57,** 327–335 (2007).

Acknowledgements

This work was supported by Grants-in-Aid from the Ministry of Education, Culture, Sports, Science, and Technology of Japan (grant numbers 21300166 to Y.K. and 22240056 to K.N.), by the Japan Society for the Promotion of Science through the "Funding program for Next Generation World-Leading Researches (NEXT Program)" initiated by the Council for Science and Technology Policy, by Shiseido Female Researcher Science Grant, Uehara Memorial Foundation, Okayama Medical Foundation, Suzuken Memorial Foundation and by a Takeda Science Foundation grant to Y.K.

Author contributions

Y.K. planned and designed the study, performed the experiments, and wrote the paper. K.I., Y.U., S.T., K.N., M.K., A.S., T.T., K.K., and S.M. carried out the experiments and analysed data. K.N. gave conceptual advice.

Additional information

Supplementary Information accompanies this paper at http://www.nature.com/naturecommunications

Competing financial interests: The authors declare no competing financial interests.

Reprints and permission information is available online at http://npg.nature.com/reprintsandpermissions/

How to cite this article: Katanosaka, Y. *et al.* TRPV2 is critical for the maintenance of cardiac structure and function in mice. *Nat. Commun.* 5:3932 doi: 10.1038/ncomms4932 (2014).

Molecular Genetics and Metabolism Reports 1 (2014) 249–253

Contents lists available at ScienceDirect

Molecular Genetics and Metabolism Reports

journal homepage: http://www.journals.elsevier.com/molecular-genetics-and-metabolism-reports/

Short Communication

Peripheral leukocyte anomaly detected with routine automated hematology analyzer sensitive to adipose triglyceride lipase deficiency manifesting neutral lipid storage disease with myopathy/triglyceride deposit cardiomyovasculopathy

Akira Suzuki [a,1], Hironori Nagasaka [b,1], Yasuhiro Ochi [c], Kazuhiro Kobayashi [d], Hiroshi Nakamura [e], Daisaku Nakatani [a], Satoshi Yamaguchi [a], Shinobu Yamaki [f], Atsushi Wada [c], Yoshihisa Shirata [g], Shu-Ping Hui [f], Tatsushi Toda [d], Hiroshi Kuroda [h], Hitoshi Chiba [f,*], Ken-ichi Hirano [a,**]

[a] *Laboratory of Cardiovascular Disease, Novel, Non-invasive, and Nutritional Therapeutics (CNT), Graduate School of Medicine, Osaka University, Suita, Osaka 565-0874, Japan*
[b] *Department of Pediatrics, Takarazuka City Hospital, Takarazuka 665-0827, Japan*
[c] *Scientific Affairs, Sysmex Corporation, Kobe 651-2241, Japan*
[d] *Division of Neurology/Molecular Brain Science, Kobe University Graduate School of Medicine, Kobe 650-0017, Japan*
[e] *Department of Community Health and Medicine, Yamaguchi University, School of Medicine, Ube 755-8505, Japan*
[f] *Faculty of Health Sciences, Hokkaido University, Sapporo 060-0812, Japan*
[g] *Sapporo Branch, Sysmex Corporation, Sapporo 060-0002, Japan*
[h] *Department of Neurology, Tohoku University Graduate School of Medicine, Sendai, 980-8574, Japan*

ARTICLE INFO

Article history:
Received 13 November 2013
Received in revised form 5 May 2014
Accepted 5 May 2014
Available online 27 May 2014

ABSTRACT

Adipose triglyceride lipase (ATGL) deficiency manifesting neutral lipid storage disease with myopathy/triglyceride deposit cardiomyovasculopathy presents distinct fat-containing vacuoles known as Jordans' anomaly in peripheral leucocytes. To develop an automatic notification system for Jordans' anomaly in ATGL-deficient

Abbreviations: ATGL, adipose triglyceride lipase; NLSD-M, Neutral lipid storage disease with myopathy (NLSD-M); TGCV, triglyceride deposit cardiomyovasculopathy.

* Corresponding author. Fax: +81 11 706 3698.
** Correspondence to: K. Hirano, Laboratory for Cardiovascular Disease, Novel, Non-invasive, and Nutritional Therapeutics (CNT) and Department of Cardiovascular Medicine, Graduate School of Medicine, Osaka University, 6-2-3, Furuedai, Suita, Osaka 565-0874, Japan. Fax: +81 6 6872 8219.
E-mail addresses: chibahit@med.hokudai.ac.jp (H. Chiba), khirano@cnt-osaka.com (K. Hirano).
[1] Authors with equal contribution: Akira Suzuki and Hironori Nagasaka.

http://dx.doi.org/10.1016/j.ymgmr.2014.05.001

Keywords:
Adipose triglyceride lipase deficiency
Automated hematology analyzer
BASO-WX and BASO-WY
Circulatory neutrophils
Jordans' anomaly
Triglyceride deposit cardiomyovasculopathy

patients, we analyzed circulatory leukocyte scattergrams on automated hematology analyzer XE-5000. The BASO-WX and BASO-WY values were found to be significantly higher in patients than those in non-affected subjects. The two parameters measured by automated hematology analyzer may be expected to provide an important diagnostic clue for homozygous ATGL deficiency.

1. Introduction

Adipose triglyceride lipase (ATGL, EC 3.1.1.3) deficiency is caused by mutations in ATGL gene, also called *PNPLA2* [1–3]. It presents profound lipid accumulation mainly in skeletal and cardiac muscles, manifesting neutral lipid storage disease with myopathy (NLSD-M)/triglyceride deposit cardiomyovasculopathy (TGCV) [3–7]. Only up to 40 patients have been reported globally [3–13]. Most of the reported cases were diagnosed in adulthood except for one case each in childhood and adolescence [12,13]. In adulthood, the myopathy and cardiomyopathy can be severe and rapidly progressive, and refractory to various therapies. Affected patients with ATGL deficiency exclusively exhibit persistent lipid droplets in the cytoplasm of circulatory neutrophils known as Jordans' anomaly (Fig. 1A) [3–13]. In earlier life, clinical symptoms seem to be absent or minimal in most cases, however Jordans' anomaly has been documented in subclinical or preclinical adolescents with ATGL deficiency [12,13]. Blood smear examination with May-Giemsa staining has been used for the detection of vacuoles in leucocytes. This report concerns a simple, easy and feasible laboratory test using a routine automated hematological analyzer that detects leukocyte abnormalities in patients with myopathy or cardiomyovasculopathy and possibly leads to a diagnosis of homozygous ATGL deficiency.

2. Methods

2.1. Subjects and specimens

Four homozygous ATGL-deficient patients (3 males and 1 female, 45–60 years of age) (Table 1) and nine heterozygous family members (4 males and 5 females, 17–83 years), lacking ATGL deficiency-associated symptoms, were enrolled. The diagnosis of ATGL deficiency was based on gene analyses together with clinical manifestations of myopathy, including easy fatigability, reduced exercise capability and limb weakness, and cardiomyopathy. Forty-three healthy subjects (14 males and 29 females, 32–84 years) lacking the mutations in ATGL gene and having no abnormality under the physical examination were also enrolled as controls. The peripheral blood specimens were collected with EDTA. Written informed consent was obtained from the enrolled subjects before study initiation.

2.2. Sample analysis

Blood specimens were analyzed by the XE-5000 automated hematology analyzer (Sysmex, Kobe, Japan) and investigated all the parameters including WBC/BASO channel of the XE-5000 to screen for Jordans' anomaly. In the WBC/BASO channel, its hemolyzing reagent, Stromatolyzer FB (Sysmex), lyses plasma membranes of cells other than basophils in the specimen and, as a result, the cytosolic components of non-basophils are released from the cells. Lipid droplets released from ATGL-deficient leukocytes which retain their shape in aqueous environment due to their own lipid monolayer membranes can be detected as smaller particles [14]. Thus, in the WBC/BASO scattergram, almost intact basophils, nucleus of

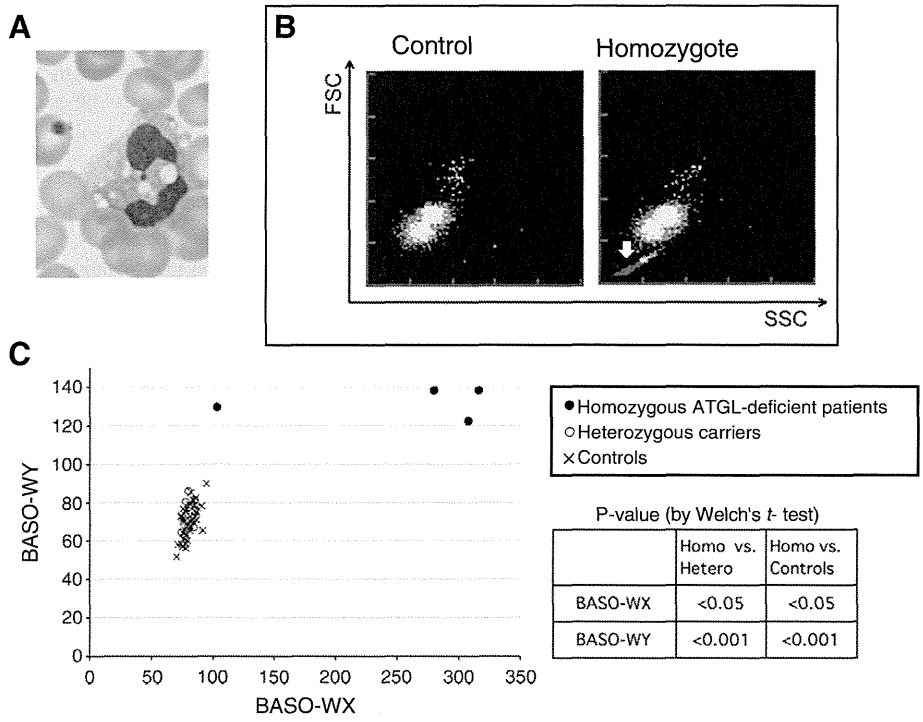

Fig. 1. (A) A representative image of May-Giemsa staining of blood smears from ATGL-deficient patients. Lipid droplets in peripheral leucocytes known as Jordans' anomaly were found in the neutrophils from all the ATGL-deficient patients. (B) Typical BASO scattergrams of control's blood (left) or homozygote's blood (right). Horizontal (X) and vertical (Y) axes indicate side and forward scattered light intensity, respectively. Colors indicate basophils (white dots), degenerated white blood cells (pale blue dots), and the other small particles (blue dots, white arrow). In these samples, BASO-WX and BASO-WY values are 79.5 and 60.3 (left, healthy), or 362.9 and 139.5 (right, patients), respectively. (C) Scatter plot of BASO-WX and BASO-WY. BASO-WX/BASO-WY values for ATGL-deficient patients (●), heterozygous ATGL carriers (○), controls (X). BASO-WX/BASO-WY values for ATGL-deficient patients were significantly higher than in other groups in Welch's *t*-test.

non-basophil leukocytes, and relatively large cytosolic components including lipid droplets or debris are detected as particles (Fig. 1B). Parameters named BASO-WX and BASO-WY, which stand for the spread of particle distribution in side and forward scattered light, respectively, are calculated in the WBC/BASO channel.

Table 1
Backgrounds of four adipose triglyceride lipase-deficient patients.

Case	Sex	Gene mutations	Reference	Present age	Cardiac function	Skeletal myopathy	Age at diagnosis[a] (Jordan's anomaly)
1	M	c.865C>T	6	50	NYHA4	Mild	41
2	M	c.696+1G>C	8	47	NYHA4	Mild	33
3	F	477_478dupCTCC	4	45	NYHA1	Severe	31
4	M	c.576delC	11	60	NYHA3	Mild	58

[a] All patients showed Jordans' anomaly in their blood smears at the diagnoses.

2.3. Statistical analysis

An analysis of Welch's *t*-test was performed to compare differences in BASO-WX and BASO-WY values between homozygous and heterozygous or controls. $p < 0.05$ was set to be statistically significant.

3. Results and discussion

After confirming that all the specimens from the four ATGL-deficient patients had Jordans' anomaly by examining their blood smears stained with May-Giemsa (Fig. 1A), we investigated all the parameters of the XE-5000 automated hematology analyzer to find any change corresponding to Jordans' anomaly. The WBC/BASO scattergram revealed an increased number of small particles in the homozygous patients, typically shown as the blue dots in Fig. 1B (white arrow in the right panel). Such change was not observed in the controls (Fig. 1B left) and in the heterozygote carriers (data not shown). The observed small particles are supposed to be the lipid droplets released from the patients' leukocytes, because lipid droplets can be expected to retain their spherical forms with neutral lipid core and phospholipid monolayer surface in this aqueous environment [14]. The BASO-WX and BASO-WY values obtained from the WBC/BASO channel of XE-5000 were significantly higher in the ATGL-deficient patients than those in the non-affected heterozygotes and the controls (Fig. 1C): 251.8 ± 100/132.0 ± 7.7 (BASO-WX/BASO-WY, mean ± SD) for the ATGL-deficient patients, 80.2 ± 3.8/74.8 ± 8.2 for the heterozygous carriers, and 80.4 ± 5.5/70.3 ± 8.2 for the controls.

We, therefore, anticipate that detection of the leucocyte abnormality in a routine automated hematological analysis may be a first step toward the diagnosis of homozygous ATGL deficiency. We further suggest that detected positive subjects should undergo more detailed analyses, including ATGL gene analyses, to establish the diagnosis in the clinical practice.

In homozygous ATGL deficiency, once the clinical presentations of myopathy and cardiomyopathy occur, it has been difficult so far to regress or resolve symptoms through any conventional treatments [3–12]. We reported two patients with severe cardiomyovasculopathy and heart failure requiring cardiac transplantation [6,8]. We recently provided data indicating that up-regulation of peroxisome proliferated activated receptor-γ and the related genes may promote triglyceride accumulation in the skeletal and cardiac muscles in ATGL deficiency [8]. We believe that the development of an easy method to detect cellular triglyceride accumulation is desired. It is quite likely that the change in the leukocyte emerges before the development of myopathy or cardiomyovasculopathy, as it does in other congenital lipid storage diseases such as Gaucher's and Niemann–Pick disease, which show distinct lipid storage in circulatory and bone marrow macrophages [15].

In our settings, heterozygous carriers could not be differentiated from control subjects, even though Jordans' anomaly has been reported in some heterozygous ATGL deficiency [16]. We speculate that one of the reasons for this may be that heterozygous leukocytes may have enough ATGL enzymatic activity to reduce the number and/or size of intracellular lipid droplets, so that BASO-WX and BASO-WY parameters were not different between heterozygous and control subjects.

It has been known that Jordans' anomaly in leukocytes is present not only in ATGL deficiency but also in Chanarin–Dorfman syndrome also called NLSD with ichthyosis, which is caused by deficiency of the protein CGI-58, an activator of the ATGL enzyme [17,18]. Further, in carnitine palmitoyltransferase deficiency type 1, a fatty acid beta-oxidation disorder engendering hypoglycemia and acidosis, this anomaly can sometimes be found in blood smears [19]. It would be of interest to know whether the present system can detect leucocyte abnormalities in these disorders, even we did not have the chance to test the possibility because of the disease rarity.

The sensitivity and specificity of BASO-WX and BASO-WY for ATGL deficiency remains to be investigated, however we believe that this automatic detection of changes in leukocytes with an automated hematology analyzer may provide an earlier diagnostic clue for ATGL deficiency to clinicians, who encounter patients with neuromuscular and cardiovascular disorders, whose causes are unknown.

In order to increase information on the natural history and pathophysiology in NLSD/TGCV patients, we have started an international registry system on the web (http://www.tgcv.org/r/home.html).

4. Conclusions

The BASO-WX and BASO-WY values obtained from automated hematology analyzer XE-5000 could help to detect Jordans' anomaly. A notification system using an automated hematology analyzer may prompt the earlier and easier diagnosis of homozygous ATGL deficiency.

Acknowledgments

The authors would like to thank Dr. Toshimitsu Hamasaki for giving us valuable advice on statistical analysis. This work is supported by a research grant for rare and intractable diseases from the Ministry of Health, Labour, and Welfare of Japan. Y.O., A.W. and Y.S. are employees of Sysmex Corporation.

References

[1] C. Bruno, S. Dimauro, Lipid storage myopathies, Curr. Opin. Neurol. 21 (2008) 601–606, http://dx.doi.org/10.1097/WCO.0b013e32830dd5a6.
[2] P. Laforêt, C. Vianey-Saban, Disorders of muscle lipid metabolism: diagnostic and therapeutic challenges, Neuromuscul. Disord. 20 (2010) 693–700, http://dx.doi.org/10.1016/j.nmd.2010.06.018.
[3] J. Fischer, C. Lefèvre, E. Morava, J.M. Mussini, P. Laforêt, A. Negre-Salvayre, M. Lathrop, R. Salvayre, The gene encoding adipose triglyceride lipase (PNPLA2) is mutated in neutral lipid storage disease with myopathy, Nat. Genet. 39 (2007) 28–30, http://dx.doi.org/10.1038/ng1951.
[4] M. Akiyama, K. Sakai, M. Ogawa, J.R. McMillan, D. Sawamura, H. Shimizu, Novel duplication mutation in the patatin domain of adipose triglyceride lipase (PNPLA2) in neutral lipid storage disease with severe myopathy, Muscle Nerve 36 (2007) 856–859, http://dx.doi.org/10.1002/mus.20869.
[5] K. Kobayashi, T. Inoguchi, Y. Maeda, N. Nakashima, A. Kuwano, E. Eto, N. Ueno, S. Sasaki, F. Sawada, M. Fujii, Y. Matoba, S. Sumiyoshi, H. Kawate, R. Takayanagi, The lack of the C-terminal domain of adipose triglyceride lipase causes neutral lipid storage disease through impaired interactions with lipid droplets, J. Clin. Endocrinol. Metab. 93 (2008) 2877–2884, http://dx.doi.org/10.1210/jc.2007-2247.
[6] K. Hirano, Y. Ikeda, N. Zaima, Y. Sakata, G. Matsumiya, Triglyceride deposit cardiomyovasculopathy, N. Engl. J. Med. 359 (2008) 2396–2398, http://dx.doi.org/10.1056/NEJMc0805305.
[7] K. Hirano, A novel clinical entity: triglyceride deposit cardiomyovasculopathy, J. Atheroscler. Thromb. 16 (2009) 702–705, http://dx.doi.org/10.5551/jat.1669.
[8] K. Hirano, T. Tanaka, Y. Ikeda, S. Yamaguchi, N. Zaima, K. Kobayashi, A. Suzuki, Y. Sakata, Y. Sakata, K. Kobayashi, T. Toda, N. Fukushima, H. Ishibashi-Ueda, D. Tavian, H. Nagasaka, S.P. Hui, H. Chiba, Y. Sawa, M. Hori, Genetic mutations in adipose triglyceride lipase and myocardial up-regulation of peroxisome proliferated activated receptor-gamma in patients with triglyceride deposit cardiomyovasculopathy, Biochem. Biophys. Res. Commun. 443 (2014) 574–579, http://dx.doi.org/10.1016/j.bbrc.2013.12.003.
[9] P. Reilich, R. Horvath, S. Krause, N. Schramm, D.M. Turnbull, M. Trenell, K.G. Hollingsworth, G.S. Gorman, V.H. Hans, J. Reimann, A. MacMillan, L. Turner, A. Schollen, G. Witte, B. Czermin, E. Holinski-Feder, M.C. Walter, B. Schoser, H. Lochmüller, The phenotypic spectrum of neutral lipid storage myopathy due to mutations in the PNPLA2 gene, J. Neurol. 258 (2011) 1987–1997, http://dx.doi.org/10.1007/s00415-011-6055-4.
[10] D. Tavian, S. Missaglia, C. Redaelli, E.M. Pennisi, G. Invernici, R. Wessalowski, R. Maiwald, M. Arca, R.A. Coleman, Contribution of novel ATGL missense mutations to the clinical phenotype of NLSD-M: a strikingly low amount of lipase activity may preserve cardiac function, Hum. Mol. Genet. 21 (2012) 5318–5328, http://dx.doi.org/10.1093/hmg/dds388.
[11] K. Kaneko, H. Kuroda, R. Izumi, M. Tateyama, M. Kato, K. Sugimura, Y. Sakata, Y. Ikeda, K. Hirano, M. Aoki, A novel mutation in PNPLA2 causes neutral lipid storage disease with myopathy and triglyceride deposit cardiomyovasculopathy: a case report and literature review. Neuromuscul. Disord. (in press). http://dx.doi.org/10.1016/j.nmd.2014.04.001 .
[12] H.O. Akman, G. Davidzon, K. Tanji, E.J. Macdermott, L. Larsen, M.M. Davidson, R.G. Haller, L.S. Szczepaniak, T.J. Lehman, M. Hirano, S. DiMauro, Neutral lipid storage disease with subclinical myopathy due to a retrotransposal insertion in the PNPLA2 gene, Neuromuscul. Disord. 20 (2010) 397–402, http://dx.doi.org/10.1016/j.nmd.2010.04.004.
[13] L. Perrin, L. Féasson, A. Furby, P. Laforêt, F.M. Petit, V. Gautheron, S. Chabrier, PNPLA2 mutation: a paediatric case with early onset but indolent course, Neuromuscul. Disord. 23 (2013) 986–991, http://dx.doi.org/10.1016/j.nmd.2013.08.008.
[14] K. Tauchi-Sato, S. Ozeki, T. Houjou, R. Taguchi, T. Fujimoto, The surface of lipid droplets is a phospholipid monolayer with a unique fatty acid composition, J. Biol. Chem. 277 (2002) 44507–44512, http://dx.doi.org/10.1074/jbc.M207712200.
[15] R.Y. Wang, O.A. Bodamer, M.S. Watson, W.R. Wilcox, ACMG Work Group on Diagnostic Confirmation of Lysosomal Storage Diseases: diagnostic confirmation and management of presymptomatic individuals, Genet. Med. 13 (2011) 457–484, http://dx.doi.org/10.1097/GIM.0b013e318211a7e1.
[16] M.C. Janssen, B. van Engelen, L. Kapusta, M. Lammens, M. van Dijk, J. Fischer, M. van der Graaf, R.A. Wevers, M. Fahrleitner, R. Zimmermann, E. Morava, Symptomatic lipid storage in carriers for the PNPLA2 gene, Eur. J. Hum. Genet. 21 (2013) 807–815, http://dx.doi.org/10.1038/ejhg.2012.256.
[17] C. Lefèvre, F. Jobard, F. Caux, B. Bouadjar, A. Karaduman, R. Heilig, H. Lakhdar, A. Wollenberg, J.L. Verret, J. Weissenbach, M. Ozguc, M. Lathrop, J.F. Prud'homme, J. Fischer, Mutations in CGI-58, the gene encoding a new protein of the esterase/lipase/thioesterase subfamily, in Chanarin–Dorfman syndrome, Am. J. Hum. Genet. 69 (2001) 1002–1012, http://dx.doi.org/10.1086/324121.
[18] C. Bruno, E. Bertini, M. Di Rocco, D. Cassandrini, G. Ruffa, T. De Toni, M. Seri, M. Spada, G. Li Volti, A. D'Amico, F. Trucco, M. Arca, C. Casali, C. Angelini, S. Dimauro, C. Minetti, Clinical and genetic characterization of Chanarin–Dorfman syndrome, Biochem. Biophys. Res. Commun. 369 (2008) 1125–1128, http://dx.doi.org/10.1016/j.bbrc.2008.03.010.
[19] J.P. Bonnefont, F. Demaugre, C. Prip-Buus, J.M. Saudubray, M. Brivet, N. Abadi, L. Thuillier, Carnitine palmitoyltransferase deficiencies, Mol. Genet. Metab. 68 (1999) 424–440, http://dx.doi.org/10.1006/mgme.1999.2938.

Molecular Genetics and Metabolism Reports 1 (2014) 264–268

Contents lists available at ScienceDirect

Molecular Genetics and Metabolism Reports

journal homepage: http://www.journals.elsevier.com/molecular-genetics-and-metabolism-reports/

Short Communication

Disease-associated marked hyperalphalipoproteinemia

Ken-ichi Hirano [a,*,1], Hironori Nagasaka [b,1], Kazuhiro Kobayashi [c], Satoshi Yamaguchi [a], Akira Suzuki [a], Tatsushi Toda [c], Manabu Doyu [d]

[a] Laboratory of Cardiovascular Disease, Novel, Non-invasive, and Nutritional Therapeutics (CNT), Graduate School of Medicine, Osaka University, Osaka 565-0874, Japan
[b] Department of Pediatrics, Takarazuka City Hospital, Takarazuka, Hyogo 665-0827, Japan
[c] Division of Neurology/Molecular Brain Science, Kobe University Graduate School of Medicine, Kobe 650-0017, Japan
[d] Department of Neurology, Aichi Medical University, Aichi 480-1195, Japan

ARTICLE INFO

Article history:
Received 4 May 2014
Received in revised form 3 June 2014
Accepted 3 June 2014
Available online 30 June 2014

Keywords:
Atherosclerosis
Cardiovascular disease
Cholesteryl ester transfer protein deficiency
High density lipoprotein
Hyperalphalipoproteinemia
Stroke

ABSTRACT

Marked hyperalphalipoproteinemia (HAL) is a heterogeneous syndrome. To clarify the pathophysiological significance of HAL, we compared clinical profiles between marked HAL subjects with and without cholesteryl ester transfer protein (CETP) deficiency. CETP deficiency was associated with cardiovascular diseases and strokes in the HAL population, particularly in female. HAL women without CETP deficiency tended to have higher prevalence with cancer history. HAL may not always be a longevity marker, but be sometimes accompanied with pathological conditions.

1. Introduction

Hyperalphalipoproteinemia (HAL) had been regarded as a longevity syndrome. Matsuzawa et al. reported that a man with HAL unexpectedly had a corneal opacity which is a clinical sign for high density lipoprotein (HDL) deficiency [1]. Following studies revealed that genetic deficiency of cholesteryl ester transfer protein (CETP) is a major cause for HAL in Japan [2,3]. CETP is a plasma glycoprotein which facilitates the transfer of cholesteryl ester from HDL to apolipoprotein

* Corresponding author at: Laboratory for Cardiovascular Disease, Novel, Non-invasive, and Nutritional Therapeutics (CNT) and Department of Cardiovascular Medicine, Graduate School of Medicine, Osaka University, 6-2-3, Furuedai, Suita, Osaka 565-0874, Japan. Fax: +81 6 6872 8219.
E-mail addresses: khirano@cnt-osaka.com, khirano@cardiology.med.osaka-u.ac.jp (K. Hirano).
[1] These authors equally contributed to this work.

http://dx.doi.org/10.1016/j.ymgmr.2014.06.001

B-containing lipoproteins, then determine the plasma levels of HDL-cholesterol and low-density lipoprotein (LDL)-cholesterol levels [4]. This protein also regulates the lipid composition and particle size of lipoproteins.

CETP deficiency presents marked HAL and relative decrease in LDL-cholesterol level [5]. Such lipid profiles are generally believed protective for cardiovascular diseases (CVDs) and strokes, however, there has been a controversy whether this genetic deficiency is overall anti- or pro-atherogenic [6–8]. In addition, it is noteworthy that some clinical trials with CETP inhibitors recently failed and terminated [9], suggesting that further understanding pathophysiological significance for HAL is obviously required.

Here, we examined the prevalence of CVDs and strokes in HAL subjects with and without CETP deficiency along with their respective lipid profiles in a specific community, Akita Prefecture, Japan, where we reported that genetic CETP deficiency accumulates [10].

2. Subjects and methods

2.1. Subjects

The surveyed population comprised residents aged over 20-years-old in a community in Daisen City, Akita Prefecture, Japan (http://www.city.daisen.akita.jp/content/docs/english/), which includes Omagari area where genetic CETP deficiency accumulates [9,10].

After the opt-out in the community journal, we directly sent a request letter to 343 people with marked HAL (HDL-C > 100 mg/dL) based upon the annual health examination for the last three years. Unrelated 181 individuals (53%) agreed to participate in this study. Physical examination, blood test, and interview for medical histories and records of CVDs and strokes were performed. Based upon the analyses of the CETP gene and the protein levels, the subjects with HAL were divided into CETP-deficient and non-CETP-deficient groups.

This study was approved by the ethical committee in Osaka University.

2.2. Medical interview

We performed interviews on smoking, alcohol consumption, and medical histories for CVDs, stroke, diabetes mellitus, hypertension, hyperlipidemia, and cancer.

Diagnoses of hypertension and diabetes mellitus were made according to the criteria of Japanese Society of Hypertension and Japan Diabetes Society. CVDs include non-fatal myocardial infarction, angina pectoris, congestive heart failure, and arteriosclerosis obliterans. Strokes include cerebral infarction and cerebral hemorrhage, but exclude subarachnoid hemorrhage and strokes associated with atrial fibrillation. Cancers included any malignant tumors treated previously and currently.

2.3. CETP gene analyses

We performed direct sequencing of the DNA fragments amplified by polymerase chain reaction to detect two common CETP gene mutations [11,12]: intron 14 splicing defect (c.1321 + 1G>A, rs5742907) and missense mutation in exon 15 (c.1376A>G, rs2303790).

2.4. CETP protein mass

CETP protein mass was measured by the commercial available ELISA kit according to the manufacturer's protocol [13,14].

2.5. Criteria for CETP deficiency

Criteria of CETP deficiency was one of the following: 1) either of the common genetic mutations with c.1321 + 1G>A or c.1376A>G. We previously reported that these two CETP gene mutations contributed to approximately 90% of the genetic CETP deficiency in Japan (13, 14); 2) CETP mass was below 2.0 μg/mL.

We decided to use this cut-off value because the mean CETP mass level of the heterozygote for the missense mutation in exon 15 was 1.65 ± 0.31 μg/mL, as reported by Goto et al. [14].

2.6. Lipoproteins analyses

Serum lipoproteins were analyzed by analytical HPLC service system (LipoSEARCH®) at Skylight Biotech Inc. (Akita, Japan), as previously described [15].

2.7. Statistical methods

Data are presented as means (SD). All pair-wise comparisons between CETP- and non-CETP deficient groups were performed with the two-sided Student's *t*-test, and differences in percent values between these two groups were examined by Fisher's exact test. p Values < 0.05 were considered significant.

3. Results

Among the 181 participants with marked HAL, the numbers of CETP-deficient and non-CETP-deficient subjects were 71 and 110, respectively. There were no statistical significance of age and listed coronary risk factors, including hypertension, diabetes mellitus, and cigarette smoking (Table 1).

Among 71 CETP-deficient subjects, 2 were revealed to be homozygous. Prevalence of CVDs history was significantly higher in CETP-deficient group than in non-CETP-deficient group ($p = 0.016$). Particularly in female subgroups, the prevalence of CVDs and strokes was significantly higher in CETP-deficient female ($p = 0.02$ for CVD, $p = 0.028$ for ischemic stroke) (Table 1). Furthermore, the prevalence of cancer history tended to be higher in non-CETP-deficient females than in CETP-deficient ones, although not significant statistically (Table 1). Among HAL women without CETP deficiency, the histories for gastric and uterine/breast cancers seem to be higher.

The particle sizes of HDL and LDL were not different significantly between CETP-deficient and non-CETP-deficient groups. HDL-TG/HDL-cholesterol ratio was significantly decreased in CETP-deficient group than non-CETP-deficient group ($p = 0.002$), whereas LDL-TG/LDL-cholesterol ratio was significantly increased in CETP-deficient group ($p = 0.01$) (Table 1), which is compatible with our previous reports [16,17].

4. Discussion

In the previous cross-sectional study in Omagari area, Japan, where CETP deficiency accumulates, we found that there was a U-shaped relationship between plasma HDL-cholesterol and ischemic electrocardiographic changes for the first time [10]. Zhong et al. reported that heterozygous CETP deficiency may be associated with CVDs in Japanese-American population in Hawaii [18], consistent with results of our previous study. Further, recent reports have drawn U-shaped relationship between plasma HDL-C levels and prevalence of CVDs in the other subjects and population [19,20]. The results of this study, together with those of previous studies, provide evidence that HAL is not always promising for the preventions of CVDs and strokes.

We and others reported that CETP deficiency results in qualitative and quantitative abnormalities in both HDL and LDL [16,17], as shown in Table 1. Triglyceride-rich LDL had lower affinity for LDL receptor [17] and may be susceptible for oxidation in plasma. There seems to be controversial whether large and cholesterol-rich HDL from CETP deficiency had reduced or improved ability for cholesterol efflux from lipid-laden macrophages, depending on their experimental settings [16,21,22].

Unexpectedly, we noticed that the cancer history tended to be more frequent in HAL without CETP deficiency than with CETP deficiency (Table 1). It is known that the Akita Prefecture has one of the highest cancer mortalities among all prefectures in Japan last couple of decades. Further study would be of significance to know the association between HAL and cancer for public health as well as medical science.

The present study has the following limitations: 1) we focused on subjects with marked HAL who voluntarily participated. Therefore, residents with some clinical problems might be more motivated to participate compared with those without any clinical problems, which might raise a possibility that the

Table 1
Clinical profiles in subjects with marked hyperalphalipoproteinemia with and without CETP deficiency.

	CETP deficiency	Non-CETP deficiency	P
Total number	71	110	
Age (y)	67 ± 12	64 ± 13	0.263
CETP mass (mg/mL)	1.7 ± 0.5	2.8 ± 0.5	0.0009
Coronary risk factors			
Hypertension	22 (31%)	36 (33%)	0.878
LDL-cholesterol (mg/dL)	98 ± 24	103 ± 29	0.284
Diabetes mellitus	4 (6%)	10 (9%)	0.572
Smoking habit	18 (26%)	29 (26%)	1.00
Triglycerides:cholesterol ratio in HDL	0.15 ± 0.03	0.21 ± 0.03	0.002
Triglycerides:cholesterol ratio in LDL	0.28 ± 0.04	0.22 ± 0.04	0.01
Cardiovascular disease	10 (14%)	3 (3%)	0.016
Stroke	5 (7%)	4 (4%)	0.487
Ischemic	5 (7%)	3 (3%)	0.271
Hemorrhagic	0 (0%	1 (1%)	1.00
Cancers	8 (11%)	19 (17%)	0.399
Gastric cancer	5 (7%)	10 (9%)	0.786
Male (n)	28	44	
Cardiovascular disease	3 (11%)	2 (5%)	0.386
Stroke	1 (4%)	4 (9%)	0.645
Ischemic	1 (4%)	3 (7%)	1.00
Hemorrhagic	0 (0%)	1 (2%)	1.00
Cancers	5 (18%)	6 (14%)	0.747
Gastric cancer	4 (14%)	5 (14%)	0.734
Others	1 (4%)	1 (4%)	1.00
Female (n)	43	66	
Cardiovascular disease	7 (16%)	1 (2%)	0.02
Stroke	4 (9%)	0 (0%)	0.028
Ischemic	4 (9%)	0 (0%)	0.028
Hemorrhagic	0 (0%)	0 (0%)	1.00
Cancers	3 (7%)	13 (20%)	0.165
Gastric cancer	1 (2%)	5 (8%)	0.404
Uterine, breast cancers	2 (5%)	7 (11%)	0.48
Others	0 (0%)	1 (2%)	1.00

Data are presented as mean ± SD (p value assessed by use of Student's *t*-test) and percentages by Fisher's exact test.
Diagnoses of hypertension and diabetes mellitus were made according to the criteria of the Japanese Society of Hypertension and the Japan Diabetes Society.
Cardiovascular diseases include non-fatal myocardial infarction, angina pectoris, congestive heart failure, and arteriosclerosis obliterans.
Stroke includes cerebral infarction and cerebral hemorrhage, and excludes subarachnoid hemorrhage and strokes associated with atrial fibrillation. Cancers include any malignant tumors treated previously and currently.

disease prevalence might be overestimated in both CETP- and non-CETP deficient HAL groups. It would be of importance to compare the disease prevalence in subjects with marked HAL with that in normolipidemic subjects in the same community; 2) we did not know the molecular basis for HAL without CETP deficiency, although molecules such as hepatic triglyceride lipase [7,22] were reported as responsible for some types of HAL.

In conclusion, marked HAL is not always beneficial for the prevention of CVDs and strokes. Rather, marked HAL may be occasionally associated with the developments of these life-threatening diseases, depending on their sexes and genetic backgrounds.

Acknowledgment

The authors would like to thank Dr. Yoshinobu Ikeda, Dr. Yoshiya Toyoshima, and Professor Mitsuyo Okazaki for their helpful comments and discussion. This study was partially supported by research grant

from rare and intractable disease (H21-Nanchi-Ippan-165) from the Ministry of Health, Labor, and Welfare, Japan.

References

[1] Y. Matsuzawa, S. Yamashita, K. Kameda, M. Kubo, S. Tarui, I. Hara, Marked hyper-HDL2-cholesterolemia associated with premature corneal opacity. A case report, Atherosclerosis 53 (1984) 207–212 (http://www.ncbi.nlm.nih.gov/pubmed/6517975).
[2] J. Koizumi, H. Mabuchi, A. Yoshimura, I. Michishita, M. Takeda, H. Itoh, Y. Sakai, T. Sakai, K. Ueda, R. Takeda, Deficiency of serum cholesteryl-ester transfer activity in patients with familial hyperalphalipoproteinaemia, Atherosclerosis 58 (1985) 175–186 (http://www.ncbi.nlm.nih.gov/pubmed/3937535).
[3] S. Yamashita, Y. Matsuzawa, M. Okazaki, H. Kako, T. Yasugi, H. Akioka, K. Hirano, S. Tarui, Small polydisperse low density lipoproteins in familial hyperalphalipoproteinemia with complete deficiency of cholesteryl ester transfer activity, Atherosclerosis 70 (1988) 7–12 (http://www.ncbi.nlm.nih.gov/pubmed/3355618).
[4] A.R. Tall, Plasma cholesteryl ester transfer protein, J. Lipid Res. 34 (1993) 1255–1274 (http://www.ncbi.nlm.nih.gov/pubmed/8409761).
[5] A. Inazu, M.L. Brown, C.B. Hesler, L.B. Agellon, J. Koizumi, K. Takata, Y. Maruhama, H. Mabuchi, A.R. Tall, Increased high-density lipoprotein levels caused by a common cholesteryl-ester transfer protein gene mutation, N. Engl. J. Med. 323 (1990) 1234–1238, http://dx.doi.org/10.1056/NEJM199011013231803.
[6] C.J. Fielding, R.J. Havel, Cholesteryl ester transfer protein: friend or foe? J. Clin. Invest. 97 (1996) 2687–2688, http://dx.doi.org/10.1172/JCI118719.
[7] K. Hirano, S. Yamashita, Y. Kuga, N. Sakai, S. Nozaki, S. Kihara, T. Arai, K. Yanagi, S. Takami, M. Menju, et al., Atherosclerotic disease in marked hyperalphalipoproteinemia. Combined reduction of cholesteryl ester transfer protein and hepatic triglyceride lipase, Arterioscler. Thromb. Vasc. Biol. 15 (1995) 1849–1856 (http://www.ncbi.nlm.nih.gov/pubmed/7583564).
[8] K. Hirano, S. Yamashita, Y. Matsuzawa, Pros and cons of inhibiting cholesteryl ester transfer protein, Curr. Opin. Lipidol. 11 (2000) 589–596 (http://www.ncbi.nlm.nih.gov/pubmed/11086331).
[9] P.J. Barter, K.A. Rye, Cholesteryl ester transfer protein inhibition as a strategy to reduce cardiovascular risk, J. Lipid Res. 53 (2012) 1755–1766, http://dx.doi.org/10.1194/jlr.R024075.
[10] K. Hirano, S. Yamashita, N. Nakajima, T. Arai, T. Maruyama, Y. Yoshida, M. Ishigami, N. Sakai, K. Kameda-Takemura, Y. Matsuzawa, Genetic cholesteryl ester transfer protein deficiency is extremely frequent in the Omagari area of Japan. Marked hyperalphalipoproteinemia caused by CETP gene mutation is not associated with longevity, Arterioscler. Thromb. Vasc. Biol. 17 (1997) 1053–1059 (http://www.ncbi.nlm.nih.gov/pubmed/9194754).
[11] T. Maruyama, N. Sakai, M. Ishigami, K. Hirano, T. Arai, S. Okada, E. Okuda, A. Ohya, N. Nakajima, K. Kadowaki, E. Fushimi, S. Yamashita, Y. Matsuzawa, Prevalence and phenotypic spectrum of cholesteryl ester transfer protein gene mutations in Japanese hyperalphalipoproteinemia, Atherosclerosis 166 (2003) 177–185 (http://www.ncbi.nlm.nih.gov/pubmed/12482565).
[12] M. Nagano, S. Yamashita, K. Hirano, M. Takano, T. Maruyama, M. Ishihara, Y. Sagehashi, T. Kujiraoka, K. Tanaka, H. Hattori, N. Sakai, N. Nakajima, T. Egashira, Y. Matsuzawa, Molecular mechanisms of cholesteryl ester transfer protein deficiency in Japanese, J. Atheroscler. Thromb. 11 (2004) 110–121 (http://www.ncbi.nlm.nih.gov/pubmed/15256762).
[13] K. Saito, K. Kobori, H. Hashimoto, S. Ito, M. Manabe, S. Yokoyama, Epitope mapping for the anti-rabbit cholesteryl ester transfer protein monoclonal antibody that selectively inhibits triglyceride transfer, J. Lipid Res. 40 (1999) 2013–2021 (http://www.ncbi.nlm.nih.gov/pubmed/10553005).
[14] A. Goto, K. Sasai, S. Suzuki, T. Fukutomi, S. Ito, T. Matsushita, M. Okamoto, T. Suzuki, M. Itoh, K. Okumura-Noji, S. Yokoyama, Cholesteryl ester transfer protein and atherosclerosis in Japanese subjects: a study based on coronary angiography, Atherosclerosis 159 (2001) 153–163 (http://www.ncbi.nlm.nih.gov/pubmed/11689217).
[15] M. Okazaki, S. Usui, A. Fukui, I. Kubota, H. Tomoike, Component analysis of HPLC profiles of unique lipoprotein subclass cholesterols for detection of coronary artery disease, Clin. Chem. 52 (2006) 2049–2053, http://dx.doi.org/10.1373/clinchem.2006.070094.
[16] M. Ishigami, S. Yamashita, N. Sakai, T. Arai, K. Hirano, H. Hiraoka, K. Kameda-Takemura, Y. Matsuzawa, Large and cholesteryl ester-rich high-density lipoproteins in cholesteryl ester transfer protein (CETP) deficiency can not protect macrophages from cholesterol accumulation induced by acetylated low-density lipoproteins, J. Biochem. 116 (1994) 257–262 (http://www.ncbi.nlm.nih.gov/pubmed/7822240).
[17] N. Sakai, S. Yamashita, K. Hirano, M. Ishigami, T. Arai, K. Kobayashi, T. Funahashi, Y. Matsuzawa, Decreased affinity of low density lipoprotein (LDL) particles for LDL receptors in patients with cholesteryl ester transfer protein deficiency, Eur. J. Clin. Invest. 25 (1995) 332–339 (http://www.ncbi.nlm.nih.gov/pubmed/7628520).
[18] S. Zhong, D.S. Sharp, J.S. Grove, C. Bruce, K. Yano, J.D. Curb, A.R. Tall, Increased coronary heart disease in Japanese-American men with mutation in the cholesteryl ester transfer protein gene despite increased HDL levels, J. Clin. Invest. 97 (1996) 2917–2923, http://dx.doi.org/10.1172/JCI118751.
[19] J.P. Corsetti, W. Zareba, A.J. Moss, D.L. Rainwater, C.E. Sparks, Elevated HDL is a risk factor for recurrent coronary events in a subgroup of non-diabetic postinfarction patients with hypercholesterolemia and inflammation, Atherosclerosis 187 (2006) 191–197, http://dx.doi.org/10.1016/j.atherosclerosis.2005.09.012.
[20] T. Costacou, R.W. Evans, T.J. Orchard, High-density lipoprotein cholesterol in diabetes: is higher always better? J. Clin. Lipidol. 5 (2011) 387–394, http://dx.doi.org/10.1016/j.jacl.2011.06.011.
[21] W. Plengpanich, W. Le Goff, S. Poolsuk, Z. Julia, M. Guerin, W. Khovidhunkit, CETP deificiency due to a novel mutation in the CETP gene promoter and its effect on cholesterol efflux and selective uptake into hepatocytes, Atherosclerosis 216 (2011) 370–373, http://dx.doi.org/10.1016/j.atherosclerosis.2011.01.051 (Epub 2011 Feb 26).
[22] P.E. Khoury, W. Plengpanich, E. Frisdal, W. Le Goff, W. Khovidhunkit, M. Guerin, Improved plasma cholesterol efflux capacity from human macrophages in patients with hyperalphalipoproteinemia, Atherosclerosis 234 (2014) 193–199, http://dx.doi.org/10.1016/j.atherosclerosis.2014.02.032 (Epub 2014 Mar 12).

Neurobiology of Disease

The Role of Pak-Interacting Exchange Factor-β Phosphorylation at Serines 340 and 583 by PKCγ in Dopamine Release

Toshihiko Shirafuji,[1] Takehiko Ueyama,[1] Ken-ichi Yoshino,[1] Hideyuki Takahashi,[1] Naoko Adachi,[1] Yukio Ago,[2] Ken Koda,[2] Tetsuaki Nashida,[2] Naoki Hiramatsu,[2] Toshio Matsuda,[2] Tatsushi Toda,[3] Norio Sakai,[4] and Naoaki Saito[1]

[1]Laboratory of Molecular Pharmacology, Biosignal Research Center, Kobe University, Kobe 657-8501, Japan, [2]Laboratory of Medicinal Pharmacology, Graduate School of Pharmaceutical Sciences, Osaka University, Suita, Osaka 565-0871, Japan, [3]Division of Neurology/Molecular Brain Science, Kobe University Graduate School of Medicine, Kobe 650-0017, Japan, and [4]Department of Molecular and Pharmacological Neuroscience, Graduate School of Biomedical Sciences, Hiroshima University, Hiroshima 734-8551, Japan

Protein kinase C (PKC) has been implicated in the control of neurotransmitter release. The AS/AGU rat, which has a nonsense mutation in PKCγ, shows symptoms of parkinsonian syndrome, including dopamine release impairments in the striatum. Here, we found that the AS/AGU rat is PKCγ-knock-out (KO) and that PKCγ-KO mice showed parkinsonian syndrome. However, the PKCγ substrates responsible for the regulated exocytosis of dopamine *in vivo* have not yet been elucidated. To identify the PKCγ substrates involved in dopamine release, we used PKCγ-KO mice and a phosphoproteome analysis. We found 10 candidate phosphoproteins that had decreased phosphorylation levels in the striatum of PKCγ-KO mice. We focused on Pak-interacting exchange factor-β (βPIX), a Cdc42/Rac1 guanine nucleotide exchange factor, and found that PKCγ directly phosphorylates βPIX at Ser583 and indirectly at Ser340 in cells. Furthermore, we found that PKC phosphorylated βPIX *in vivo*. Classical PKC inhibitors and βPIX knock-down (KD) significantly suppressed Ca^{2+}-evoked dopamine release in PC12 cells. Wild-type βPIX, and not the βPIX mutants Ser340 Ala or Ser583 Ala, fully rescued the decreased dopamine release by βPIX KD. Double KD of Cdc42 and Rac1 decreased dopamine release from PC12 cells. These findings indicate that the phosphorylation of βPIX at Ser340 and Ser583 has pivotal roles in Ca^{2+}-evoked dopamine release in the striatum. Therefore, we propose that PKCγ positively modulates dopamine release through β2PIX phosphorylation. The PKCγ-βPIX-Cdc42/Rac1 phosphorylation axis may provide a new therapeutic target for the treatment of parkinsonian syndrome.

Key words: βPIX; Cdc42; dopamine; Parkinson's disease; phosphoproteome; PKC

Introduction

Protein kinase C (PKC) is an important kinase in the enhancement of Ca^{2+}-triggered exocytosis (Iwasaki et al., 2000; Barclay et al., 2003). The PKC family consists of at least 10 subtypes and is divided into the following three subfamilies: conventional PKC (cPKC), novel PKC, and atypical PKC (Nishizuka, 1988, 1992). Among PKCs, only cPKCs (including PKCγ, which is a neuron-specific PKC isoform; Saito and Shirai, 2002) are activated by Ca^{2+} because they contain a C2 domain that specifically binds to Ca^{2+} and phosphatidylserine (PS; Murray and Honig, 2002).

The AS/AGU rat, a spontaneously occurring mutated animal that exhibits locomotor abnormalities, progressive dopaminergic (DAergic) neuronal degeneration in the substantia nigra (SN), and lower extracellular levels of dopamine (DA) in the striatum, has been used as a valuable model for parkinsonian syndrome (Payne et al., 2000). It is noteworthy that a mutation in PKCγ that leads to the early termination at the C2 domain without possessing the catalytic domain causes parkinsonian syndrome in AS/AGU rats (Craig et al., 2001). The mutation in AS/AGU rats should result in the kinase-dead form of PKCγ, but it is still unclear how the mutation causes parkinsonian symptoms.

PKC has been shown to modify exocytosis in at least three steps: (1) increased vesicle recruitment into readily releasable pools (Gillis et al., 1996; Stevens and Sullivan, 1998), (2) acceleration of fusion pore expansion (Scepek et al., 1998), and (3) changes in the kinetics of exocytosis (Graham et al., 2002). However, only the functional consequences of the phosphorylation of SNAP25 (Iwasaki et al., 2000), synaptotagmin I (Hilfiker et al., 1999), and Munc18 (Barclay et al., 2003) by PKC have been established on exocytosis *in vivo*. Furthermore, no attempts have been made to achieve a comprehensive understanding of DA exocytosis through an identification of

Received Oct. 6, 2013; revised May 18, 2014; accepted May 29, 2014.

Author contributions: N. Saito designed research; T.S., H.T., N.A., Y.A., K.K., T.N., and N.H. performed research; K.Y. contributed unpublished reagents/analytic tools; T.U., T.M., T.T., N. Sakai, and N. Saito analyzed data; T.S., T.U., and N. Saito wrote the paper.

We thank Sumio Sugano (University of Tokyo) and Yoshihide Hayashizaki (RIKEN Omics Science Center and Research Association for Biotechnology) for kindly providing the βPIX cDNA and Hiroshi Kiyonari and Kazuki Nakao (RIKEN CDB) for mice preservation.

The authors declare no competing financial interests.

Correspondence should be addressed to Naoaki Saito, 1-1 Rokkodai-cho, Nada-ku, Kobe 657-8501 Japan. E-mail: naosaito@kobe-u.ac.jp.

DOI:10.1523/JNEUROSCI.4278-13.2014

 0270-6474/14/349268-13$15.00/0

PKCγ substrates. Therefore, we attempted to identify the PKC substrates involved in exocytosis to reveal the mechanisms of regulated exocytosis.

Pak-interacting exchange factor-β (βPIX) is a Rho guanine nucleotide exchange factor (GEF) that specifically activates Rac1 and Cdc42 (Shin et al., 2002; Shin et al., 2004; Chahdi et al., 2005; Feng et al., 2006; Shin et al., 2006; ten Klooster et al., 2006; Chahdi and Sorokin, 2008). βPIX has been reported to be an essential element of the exocytotic machinery in neuroendocrine cells (Audebert et al., 2004; Momboisse et al., 2009). To date, there have been several studies on βPIX phosphorylation (Shin et al., 2002; Chahdi et al., 2005; Shin et al., 2006; Mayhew et al., 2007), but there have been no reports of the involvement of βPIX phosphorylation in DA release.

In the present study, we found that the AS/AGU rat is indeed a PKCγ-knock-out (KO) animal, and our phosphoproteome analysis using PKCγ KO mice found 10 candidates in the striatum that are phosphorylated by PKCγ. Among the 10 candidates, we demonstrated that PKCγ activated DA release through the phosphorylation of βPIX.

Materials and Methods

Antibodies. The anti-GFP antibody (Ab) and the anti-vesicular monoamine transporter 2 (VMAT2) Ab recognizing the C-terminal of mouse VMAT2 were prepared in house. The anti-PKCγ (C2-domain) monoclonal Abs specifically recognizing C2-domain of PKCγ have been described previously (Kose et al., 1990). The following Abs were purchased: anti-FLAG from Sigma-Aldrich (catalog #P2983 RRID:AB_439685); anti-βPIX (SH3 domain) from Millipore; anti-β-actin (catalog #ab66338 RRID:AB_2289239) and anti-PKCγ (N-terminal) specifically recognizing N-terminal of PKCγ from Abcam; anti-glutathione S-transferase (GST) (catalog #sc-33613 RRID:AB_647588), anti-PKCα (catalog #sc-208 RRID:AB_2168668), anti-PKCβ1 (catalog #sc-209 RRID:AB_2168968), anti-PKCβ2 (catalog #sc-210 RRID:AB_2252825), and anti-PKCγ (catalog #sc-211 RRID:AB_632234) from Santa Cruz Biotechnology; and anti-serPKC motif (catalog #2261S RRID: AB_330310), anti-βPIX (catalog #4515S RRID:AB_2274365) for immunoprecipitation (IP), and anti-postsynaptic density-95 (PSD95; catalog #2507S RRID:AB_10695259) from Cell Signaling Technology.

Production of anti-phosphoThr76, anti-phosphoSer340, anti-phosphoSer583, and anti-β2PIX Abs. The production of anti-phospho Abs was performed as described previously (Matsubara et al., 2012). For the preparation of anti-phospho-Thr76 (pT76), anti-phospho-Ser340 (pS340), and anti-phospho-Ser583 (pS583) βPIX Abs, oligopeptides corresponding to the amino acids of human βPIX containing pT76 [VSPKSG(pT)LKSPP], pS340 [SASPRM(pS)GFIYQ], and pS583 [SLGRRS(pS)LSRLE] were used as antigens, respectively. After the fifth boost, serum was collected and purified with an affinity column and the non-phospho-antigen peptide. The anti-β2PIX Ab was obtained by eluting the IgG from those that were bound to the nonphospho-Ser583 peptide column.

Animals. The AS/AGU rats were provided by R.W. Davies (Payne et al., 2000). The PKCγ-Cre knockin (KI) mouse was provided by Z.F. Chen (Ding et al., 2005). After the sixth backcross, homozygous littermates obtained by crossing the heterozygous PKCγ-Cre KI mouse were used as the PKCγ KO and wild-type (WT) mice in the studies. All animal studies were approved by the Institutional Animal Care and Use Committee and conducted according to the Kobe University Animal Experimentation Regulations.

Sample preparation and Western blot analysis. The brains from AS/AGU rats and mice were homogenized and the concentrations of the proteins were measured with a bicinchoninic acid (BCA) protein assay kit (Thermo Fisher Scientific). SDS-PAGE and immunoblot analyses were performed as described previously (Adachi et al., 2005).

Preparation of P2 synaptosomal fraction. Adult male mouse brains were collected and homogenized in ice-cold 0.32 M sucrose solution containing 1 mM phenylmethylsulfonyl fluoride, 20 μg/ml leupeptin, and a phosphatase-inhibitor cocktail (Nacalai Tesque). The total homogenate was subjected to centrifugation at 800 × *g* for 12 min at 4°C to remove the nuclei and the supernatant, which we defined as the total fraction, was further centrifuged at high speed at 22,000 × *g* for 20 min at 4°C. The pellet was used as the P2 synaptosomal fraction. To determine the efficiency of the P2 synaptosomal extraction process, we compared the amount of VMAT2 and PSD95 proteins between the total fraction and P2 synaptosomal fraction in the same amount of protein (50 μg), which was calculated using the BCA protein assay kit.

In vivo *microdialysis. In vivo* microdialysis was performed with male mice essentially as described previously (Koda et al., 2010; Ago et al., 2013). In brief, mice were anesthetized by injection of sodium pentobarbital (40 mg/kg, i.p.), and a guide cannula (one site per animal) for a dialysis probe (Eicom) was implanted stereotaxically in the dorsal striatum (anterior 0.1 mm, lateral 1.8 mm, ventral 2.2 mm relative to the bregma and skull; Franklin and Paxinos, 1997). The cannula was cemented in place with dental acrylic and the animals were maintained warm and allowed to recover from anesthesia. The active probe membrane was 1 mm in length. Two days after the surgery, the probe was perfused with Ringer's solution (147.2 mM NaCl, 4.0 mM KCl, and 2.2 mM $CaCl_2$, pH 6.0; Fuso Pharmaceutical Industries) at a constant flow rate of 1 μl/min. To prepare the Ringer's solution containing 100 mM K^+, an identical amount of sodium was replaced for maintaining isoosmolarity. Experiments were initiated after a stabilization period of 3 h. Microdialysis samples (20 μl) were collected every 20 min and were assayed for DA by high-performance liquid chromatography (HPLC) with electrochemical detection. No-net-flux microdialysis experiments were conducted in a PKCγ KO and WT mice as described previously (Justice, 1993; Chefer et al., 2005; Hewett et al., 2010). Three different concentrations of DA in Ringer's solution (C_{in} of 0, 5 and 20 nM DA) were perfused through the probe and DA in the perfusates (C_{out}) was measured in the fifth fraction following 4 fractions (equilibration period) at each applied DA concentration. A slope was calculated for the linear regression for DA applied (C_{in}) and the difference between dopamine applied and DA measured ($C_{in} - C_{out}$). The slope (extraction fraction) is an indirect measure of dopamine transporter (DAT) dynamics *in vivo* to remove extracellular DA.

Measurement of DA and DA metabolite levels in striatum. The concentrations of DA were quantified by HPLC with an electrochemical detector (ECD-100; Eicom; Kawasaki et al., 2006; Kawasaki et al., 2007). Tissue samples were homogenized in 0.2 M perchloric acid containing 100 μM EDTA and isoproterenol as an internal standard. The homogenate was centrifuged at 15,000 × *g* for 15 min at 0°C. The supernatant was filtered through a 0.22 μm membrane filter (Millipore), and then a 10 μl aliquot of the sample was injected onto the HPLC column every 30 min for the DA assay. An Eicompak SC-5ODS column (3.0 mm i.d. × 150 mm; Eicom) was used, and the potential of the graphite electrode (Eicom) was set to +750 mV against an Ag/AgCl reference electrode. The mobile phase contained 0.1 M sodium acetate/0.1 M citrate buffer, pH 3.5, 190 mg/L octanesulfonic acid, 5 mg/L EDTA, and 17% (v/v) methanol. Data were calculated by analyzing the peak area of the external standard of dopamine hydrochloride (Sigma-Aldrich).

Cell culture. COS7 and HEK293 cells were cultured in DMEM and Eagle's minimum essential medium (Nacalai Tesque), respectively, which were supplemented with 10% fetal bovine serum, penicillin (100 units/ml), and streptomycin (100 μg/ml). Nonessential amino acids (100 μM) were added for HEK293 cells. PC12 cells were cultured in DMEM containing 10% fetal bovine serum and 5% horse serum. All cells were cultured at 37°C in a humidified atmosphere containing 5% CO_2.

Construction of plasmids. WT PKCγ was cloned into pcDNA3.1 (Life Technologies) and the subdomains of PKCγ were cloned into pcDNA3.1 with GFP, as described previously (Seki et al., 2005). Human βPIX was provided by the RIKEN BioResource Center through the National BioResource Project of MEXT in Ibaraki, Japan (Ota et al., 2004). For the construction of plasmids encoding full-length β2PIX that was fused with 3xFLAG at the N terminal, β2PIX with a NotI/BamHI site that was produced by PCR was cloned into a 3xpFLAG-CMV10 vector (Sigma-Aldrich). Because the target sequence for rat βPIX knock-down (KD; sh369) was located in the coding region of βPIX, sh369-resistant β2PIX in the 3xpFLAG-CMV10 vector was made by placing 6-base silent

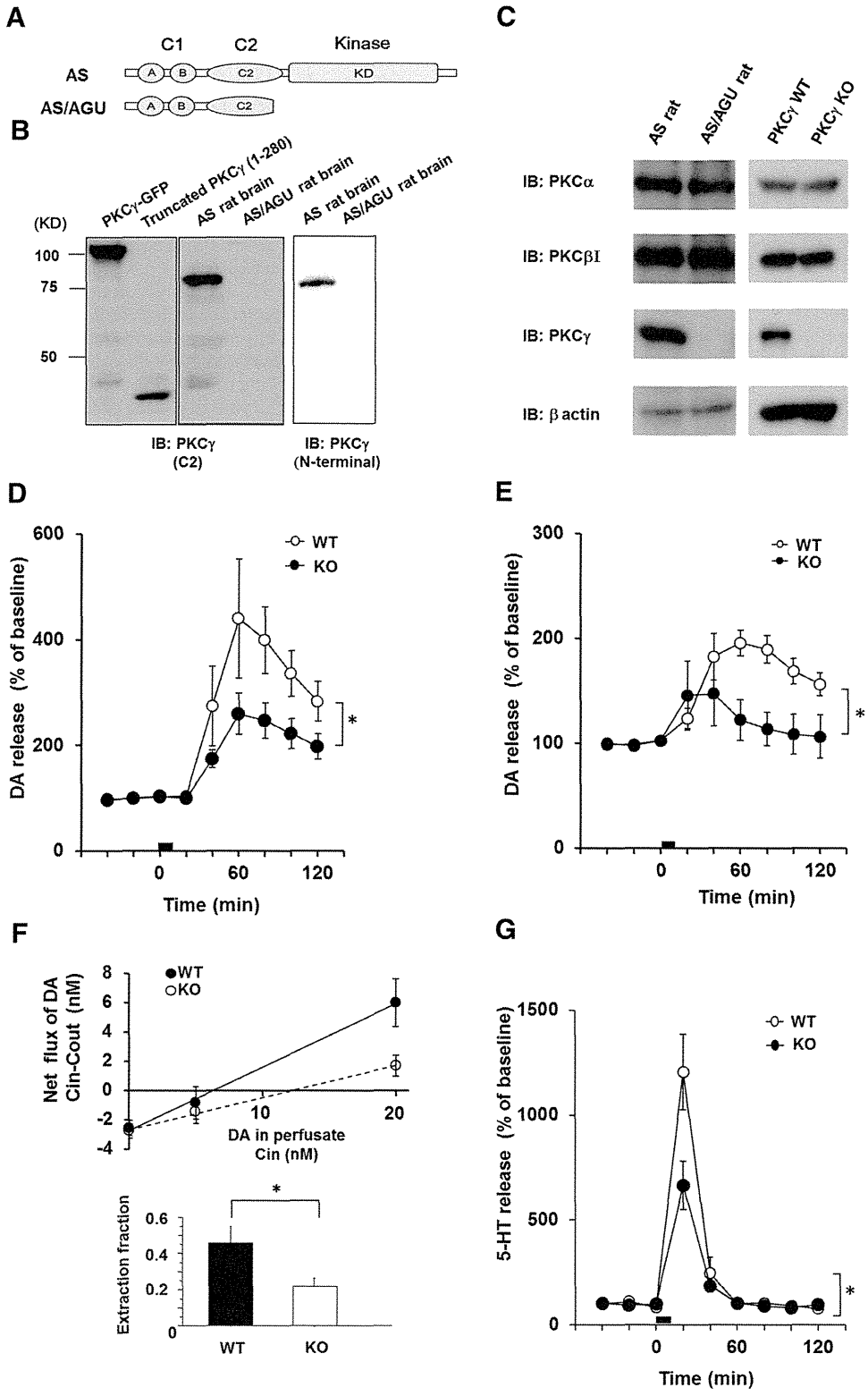

Figure 1. The PKCγ KO model exhibits symptoms of parkinsonian syndrome. ***A***, Schematic illustrations of the PKCγ protein and AS/AGU mutations. The truncated PKCγ polypeptide terminates within the C2 domain. ***B***, Recombinant truncated PKCγ (1–280 aa), which was transfected in COS-7 cells, the AS rat brain lysate, and the AS/AGU rat brain lysate, was detected by immunoblot analysis with an anti-PKCγ (C2-domain) monoclonal antibody and anti-PKCγ (N terminal) antibody, respectively. ***C***, The PKCγ KO was confirmed by immunoblot analysis of the whole brain of the AS/AGU rats and PKCγ KO mice. Arrowheads are recombinant PKCγ-GFP and PKCγ (1–280aa)-GFP, which were used as positive controls. ***D***, *In vivo* microdialysis in the striatum of the PKCγ KO mice. A high level of K^+ was perfused into the striatum through a dialysis probe for the time indicated by the square at 3–4 months. The results are expressed as mean ± SEM ($n = 4$–5, interaction of the genotype and time for DA release that was stimulated by high K^+ levels; $^*p < 0.05$, $F_{(8,48)} = 2.31$, repeated two-way ANOVA). ***E***, *In vivo* microdialysis for DA in the striatum of the PKCγ-KO (KO) mice that were stimulated with METH. METH (1 mg/kg) was perfused into the striatum through a dialysis probe for the time indicated by the square at 3 months (*Figure legend continues.*)

changes within the targeting sequence (5′-CAaACgAGtGAaAAaTTa-3′) with a QuikChange Multisite-Directed Mutagenesis Kit (Agilent Technologies). For construction of plasmids encoding full-length β2PIX or fragments that were fused to GST, full-length β2PIX and the SH3 (1–92 aa), DH (93–274 aa), and PH (275–400 aa) C-terminal (401–625 aa) regions were amplified by PCR with a Not1/BamH1 site and cloned into the pGEX-6P1 vector. Substitutions of Ser or Thr to Ala or Glu at the identified phosphorylation sites (Thr76Ala, Ser215Ala, Ser340Ala or Glu, and Ser583Ala or Glu) were introduced with a QuikChange kit.

Protein expression. Protein expression was performed as described previously (Kawasaki et al., 2010). In brief, BL21 pLys *Escherichia coli* and Sf9 cells were transformed with expression plasmids. *E. coli* and Sf9 cells were harvested and lysed. For the purification of recombinant proteins, GST-fusion proteins were purified with glutathione-Sepharose 4B resin (GE Healthcare Biosciences).

RNAi: short hairpin RNA and small interfering RNA. Double-stranded oligonucleotides were cloned into the short hairpin RNA (shRNA) expression vector, pSuper (puro; Oligoengine). The target sequence for the shRNA rat βPIX KD was 5′-GCAGACCAGCGAGAAGTTGAG-3′ (sh369; cording nucleotides 369–389). Because the βPIX shRNA sequence that we used was common to both the β1 and β2 isoforms, KDs of both β1 and β2 in PC12 cells were examined with βPIX SH3- and β2-specific antibodies. The synthesized small interfering RNA (siRNA) for rat βPIX was composed of a mixture of 4 oligonucleotides (si878: 5′-GGGAUGACAUAAAGACGUU-3′, si806: 5′-AGUGUCAAGAAGU ACGAAA-3′, si1115: 5′-GGAGCAUGAUCGAGCGCAU-3′, and si1153: 5′-CAACAGGACUUGCACGAAU-3′) was purchased from Thermo Fisher Scientific (SmartPool). Verified shRNA plasmids for KD of Cdc42 (sh197; 5′-GATTACGACCGCTGAGTTA-3′; Ueyama et al., 2014) and Rac1 (sh618; 5′-CCTTTGTACGCTTTGCTCA-3′; Ueyama et al., 2006) were described previously.

In vitro *PKC phosphorylation assay.* An *in vitro* PKC phosphorylation assay was performed as described previously (Kawasaki et al., 2010). In brief, precipitated FLAG-tagged β2PIX proteins or purified GST-tagged β2PIX were incubated with 200 ng of GST-tagged PKCγ or GST and the following buffers: 20 mM Tris, pH 7.4, 0.5 mM $CaCl_2$, 10 μM ATP, 0.5 mCi [γ-^{32}P] ATP, 8 μg/ml PS, and 0.8 μg/ml (±)-1,2-didecanoylglycerol (DO) in a 50 μl final volume. The samples were incubated with or without PKC inhibitors, including GF109203X (GFX), which was used as a pan PKC inhibitor, and Gö6976, which was used as a cPKC inhibitor, at 30°C for 15 min. For the calculation of the relative phosphorylation levels, the densitometries of the autoradiography were normalized with the total protein levels. The average relative phosphorylation levels of PKCγ stimulation were defined as 1.00.

PKC phosphorylation assay in cells. A PKC phosphorylation assay in cells was performed as described previously (Kawasaki et al., 2010) but with slight modifications. In brief, HEK293 cells were transfected with WT β2PIX in 3xpFLAG-CMV10 with a NEPA21 electroporator (Nepa Gene). After 12-O-tetradecanoylphorbol 13-acetate (TPA) stimulation with or without PKC inhibitors for 30 min in HEPES buffer at 37°C, the cells were collected and resuspended in homogenization buffer containing 150 mM NaCl, 10 mM ethylene glycol tetraacetic acid, 2 mM ethylenediamine tetracetic acid, 10 mM HEPES, pH 7.4, 1 mM phenylmethylsulfonyl fluoride, 20 μg/ml leupeptin, and a phosphatase-inhibitor cocktail. The precipitated proteins were separated by SDS-PAGE. The phosphorylated proteins were visualized with phospho-Abs. For the calculation of the relative phosphorylation levels, the densitometries of the immunoblots of the phospho-Abs were normalized to the total protein levels in each experiment and the averages of the relative levels of phosphorylation in more than three independent experiments are presented. The phosphorylation levels of the prestimulations were defined as 1.00.

PKC phosphorylation assay in vivo. The mice P2 synaptosomal fraction was resuspended in HEPES buffer containing 1 mM phenylmethylsulfonyl fluoride, 20 μg/ml leupeptin, and a phosphatase-inhibitor mixture and used for the *in vivo* PKC phosphorylation assay (Wu et al., 1982). After 2 μM TPA stimulation with or without 2 μM GFX for 30 min in HEPES buffer at 37°C, the P2 fraction was collected and resuspended in homogenization buffer containing 150 mM NaCl, 10 mM ethylene glycol tetraacetic acid, 2 mM ethylenediamine tetracetic acid, 10 mM HEPES, pH 7.4, 1 mM phenylmethylsulfonyl fluoride, 20 μg/ml leupeptin, and the phosphatase-inhibitor mixture. The precipitated proteins were separated by SDS-PAGE. The phosphorylated proteins were visualized with ser-PKC motif Abs.

DA release assay. DA release assays in βPIX KD cells were performed 96 h after transfection by NEPA21. PC12 cells were washed thrice with 500 μl of incubation solution (140 mM NaCl, 5 mM KCl, 2 mM $CaCl_2$, 1 mM $MgCl_2$, 2 mM glucose, 20 μM pargyline, and 10 mM HEPES, pH 7.5) and then incubated for 60 min in 500 μl of incubation solution with ^{3}H-DA (PerkinElmer), followed by three washes with 500 μl of incubation solution. The cells were allowed to rest or were stimulated with 500 μl of a high-K^+ solution containing 100 mM KCl and 35 mM NaCl for 10 min. The supernatant was collected and the cells were harvested in 500 μl of incubation solution with 2% Triton X-100. The amount of DA that was secreted into the medium and retained in the cells was measured in 500 μl of samples with a scintillation counter LS-6500 (Beckman Coulter). DA secretion was expressed by the following formula: %DA = (^{3}H in supernatant)/(^{3}H in supernatant + ^{3}H in cell lysate). A collagen-IV-coated six-well plate (BD Biosciences) was used for the DA release assay.

Mass spectrometry for β2PIX-phosphorylation site identification. Mass spectrometry for β2PIX-phosphorylation site identification was performed as described previously (Sakuma et al., 2012). After the *in vitro* PKC phosphorylation assay and electrophoresis, silver-stained bands that corresponded to GST-tagged β2PIX proteins were excised and destained. After reduction-alkylation reactions, the proteins in the gels were digested with porcine trypsin (sequencing grade; Promega) in 50 mM ammonium bicarbonate for 15 h at 37°C. The peptide fragments extracted from the gels were subjected to liquid chromatography/tandem mass spectrometry (LC/MS/MS) with a high-performance liquid chromatography system (Paradigm MS4; Michrom Bioresources) coupled to a linear ion trap mass spectrometer (Finnigan LTQ Orbitrap XL; Thermo Fisher Scientific). The LC/MS/MS data were interpreted with a MASCOT MS/MS ions search (Matrix Science).

Phosphoproteome analysis. Phosphoproteome analysis was performed as described previously with some modifications (Saito et al., 2006). Mice striata were dissolved in 50 mM Tris HCl, pH 9.0, 8 M urea, 10 mM ethylenediamine tetracetic acid, 1 mM phenylmethylsulfonyl fluoride, 20 μg/ml leupeptin, and a phosphatase inhibitor mixture. After homogenization with a Dounce homogenizer (10 strokes), the resultant solution was centrifuged at 2000 × *g* for 5 min and the supernatant was collected. The protein amounts were measured with a BCA protein assay kit. The proteins from the striatum were dried and resuspended in 50 mM Tris HCl buffer, pH 9.0, containing 8 M urea at a concentration of 10 μg/μl. These mixtures were subsequently reduced with dithiothreitol, alkylated with acrylamide, and digested with Lys-C endopeptidase at 37°C overnight, followed by trypsin digestion at 37°C overnight. The digested solutions were desalted and concentrated with Empore high-performance extraction disk cartridges (3M). Phosphopeptide enrichment was performed with hydroxy acid-modified metal oxide chromatography (HAMMOC; Titansphere Phos-TiO Kit; GL Sciences; Kyono et al., 2008). For elution of the phosphopeptides, 50 μl of 5% NH_3 and 5% pyrrolidine were used. The fractions were immediately acidified and desalted with SPE-C tips (GL Sciences). A Tomy CC-105 vacuum evap-

←

(Figure legend continued.) ($n = 4$, interaction of the genotype and time for DA release stimulated by METH, $F_{(8,48)} = 3.37$; $^*p < 0.01$, repeated two-way ANOVA). ***F***, No-net flux microdialysis to quantitate basal DAT activity in PKCγ KO mice. Three different concentrations of DA in CSF (0, 5, and 20 nM DA) were perfused through the probes to determine the extracellular DA concentration and extraction fraction. Linear regression for the DA perfused and DA measured provided extraction fraction (slope) as an indirect measure of DAT activity *in vivo* to remove extracellular DA. Extraction fraction for WT and KO mice are shown. Data represent mean ± SEM ($n = 4$ and 5 for WT and KO mice, respectively, $^*p < 0.05$). ***G***, *In vivo* microdialysis of serotonin in the striatum of the PKCγ-KO mice that were stimulated by high K^+ levels. K^+ (100 mM) was perfused into the striatum through a dialysis probe for the time indicated by the square at 3–4 months. The results are expressed as mean ± SEM ($n = 4$, interaction of the genotype and time for serotonin release that was stimulated by high K^+ levels, $F_{(8,48)} = 5.399$; $^*p < 0.001$, repeated two-way ANOVA).

Table 1. DA and DA metabolite levels in the striatum of PKCγ WT and KO mice

Age (mo)	Genotype	DA (ng/g weight)	DOPAC (ng/g weight)	HVA (ng/g weight)
3	KO	19629.5 ± 625.4	1838.6 ± 68.9	1490.6 ± 89.0
	WT	19516.4 ± 361.1	1999.1 ± 103.4	1652.1 ± 18.4
6	KO	20667.2 ± 803.5	1671.2 ± 113.0	1620.0 ± 93.9
	WT	17416.8 ± 781.3	1559.2 ± 77.2	1334.6 ± 63.7
12	KO	28911.0 ± 1801.4	2576.0 ± 277.9	2378.1 ± 161.3
	WT	29564.9 ± 2581.4	2253.1 ± 202.2	2392.2 ± 128.4

Results are expressed as mean ± SEM of 4–5 mice.

HVA, Homovanillic acid.

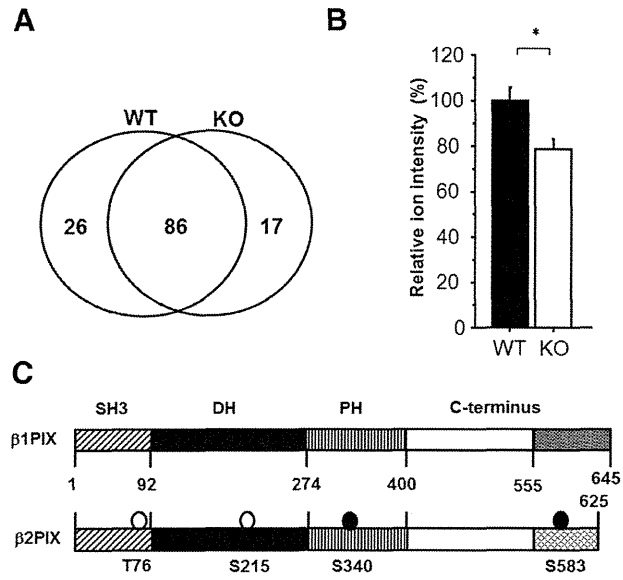

Figure 2. Phosphoproteome analysis revealed 10 phosphopeptides with decreased average ion intensity in PKCγ KO mice striatum. ***A***, Overview of the phosphoproteome (WT, $n = 5$; KO, $n = 4$). ***B***, Average ion intensity of the Ser340 βPIX phosphopeptide is calculated in both PKCγ KO and WT mice ($n = 4–5$; $^*p < 0.05$, unpaired t test). The relative average ion intensity of WT mice was defined as 100%. The results are expressed as mean ± SEM. ***C***, Schematic illustrations of the β1 and β2 PIX protein. The phosphorylation sites that were determined by the *in vitro* PKC phosphorylation assay and the phosphoproteome analysis are circled. The open circles are the phosphorylation sites that were determined only *in vitro*. The closed circles are the phosphorylation sites that were determined *in vitro* and *in vivo*.

orator was used to concentrate the sample and the phosphopeptides were analyzed by LC/MS/MS.

Statistical analysis. The data are presented as mean ± SEM and were analyzed with unpaired t tests, one-way ANOVA with a *post hoc* Dunnett's test, or a repeated two-way ANOVA. The statistical analyses were performed with the Statview 5.0J software package (SAS Institute). p-values of 5% or less were considered statistically significant.

Results

PKCγ KO animals exhibited parkinsonian symptoms, including DA release impairment in the striatum

AS/AGU rats show altered behaviors (Craig et al., 2001), DA release impairment, and the pathology of the nigrostriatal system resembles the pathology observed in human patients with parkinsonian syndrome (Campbell et al., 1996; Payne et al., 2000). AS/AGU rats have a spontaneously occurring mutation that changes the CAG (Glu281) codon to a TAG (stop codon) in PKCγ, and the putatively truncated PKCγ, if produced, will terminate at the fifth residue from the C terminus of the last strand of the β-sheet structure of the C2 domain (Fig. 1*A*). The truncated protein may result in a severe or complete loss of the kinase function of PKCγ, although it has not yet been clarified whether the truncated protein is expressed in AS/AGU rats. Although both anti-PKCγ (N terminal) Ab and anti-PKCγ (C2-domain) Ab detected an 80 kDa single band in AS rats, no band was detected in the AS/AGU rats (Fig. 1*B*). These findings indicated that PKCγ was not expressed in AS/AGU rats, suggesting the hypothesis that PKCγ KO mice show similar symptoms as those observed in AS/AGU rats. We first confirmed that our PKCγ KO mice did not express PKCγ, whereas the expression levels of other members of cPKCs were unaltered (Fig. 1*C*). To determine the effects of the PKCγ KO on DA release in the striatum, we performed *in vivo* microdialysis in the striatum. The basal line extracellular levels of DA in the striatum did not differ significantly between the PKCγ WT and KO mice. After treatment with high levels of K^+ (Fig. 1*D*) and methamphetamine (METH; Fig. 1*E*), the increase in DA release in the WT was significantly larger than that in the KO 3–4 months after birth. Although high K^+ levels induced DA release is mediated by exocytosis and not by DAT, PKC induces DAT endocytosis (Daniels and Amara, 1999), which may decrease the extracellular DA levels by increasing

Table 2. List of phosphopeptides with a PKC phosphorylation motif

Protein name	Accession no.	Sequence	Site	No. of phosphopeptides		Lowest peptide score		Highest peptide score		Average ion intensity		
				WT	KO	WT	KO	WT	KO	WT	KO	WT/KO
Gap junction alpha-1 protein	NP 034418	KVAAGHELQPLAIVDQRPSSRA	S365	7	0	11	—	28	—	3	0.4	7.3
Disks large-associated protein 1	NP 808307	RSLDSLDPAGLLTSPKF	S437	5	0	48	—	77	—	3.4	0.8	4.4
MAP kinase-activating death domain protein	NP 001171190	RATLSDSEIETNSATSAIFGKA	T1235	8	4	40	26	90	58	3.7	1	3.9
DnaJ homolog subfamily C member 5	NP 001258513	RSLSTSGESLYHVLGLDKN	S10	54	55	3	4	88	85	969	299.5	3.2
Calnexin	NP 001103969	KAEEDEILNRSPRN	S582	6	2	25	22	31	34	3.1	1.8	1.8
Stathmin	NP 062615	KRASGQAFELILSPRS	S16	26	23	8	6	93	84	12.1	7.5	1.6
Stathmin	NP 062615	RASGQAFELILSPRS	S25	25	17	5	19	81	83	7.4	5.9	1.3
Rho guanine nucleotide exchange factor 7	NP 001106989	RMSGFIYQGKL	S340	3	0	24	—	59	—	1.8	1.4	1.4
Reticulon-4	NP 077188	RRGSGSVDETLFALPAASEPVIPSSAEKI	S165	15	8	34	41	70	59	2.3	1.7	1.3
α-adducin	NP 001019629	KFRTPSFLKK	S724	3	2	7	9	29	25	6.1	4.8	1.3
β-adducin	NP 001258786	KDIATEKPGSPVKS	S594	10	8	10	17	50	56	0.4	0.3	1.2

Phosphopeptides with a WT/KO ratio >1.0 are listed. The numbers of phosphorylation sites are based on the results of mice in PhosphoSitePlus (www.phosphosite.org). S and T are the identified phosphorylation sites. Number of phosphopeptides means the total numbers of the phosphopeptides in each group ($n = 4$). Highest or lowest peptide score means the highest or lowest peptide score in each group ($n = 4$). Peptides that were not detected are shown as —.

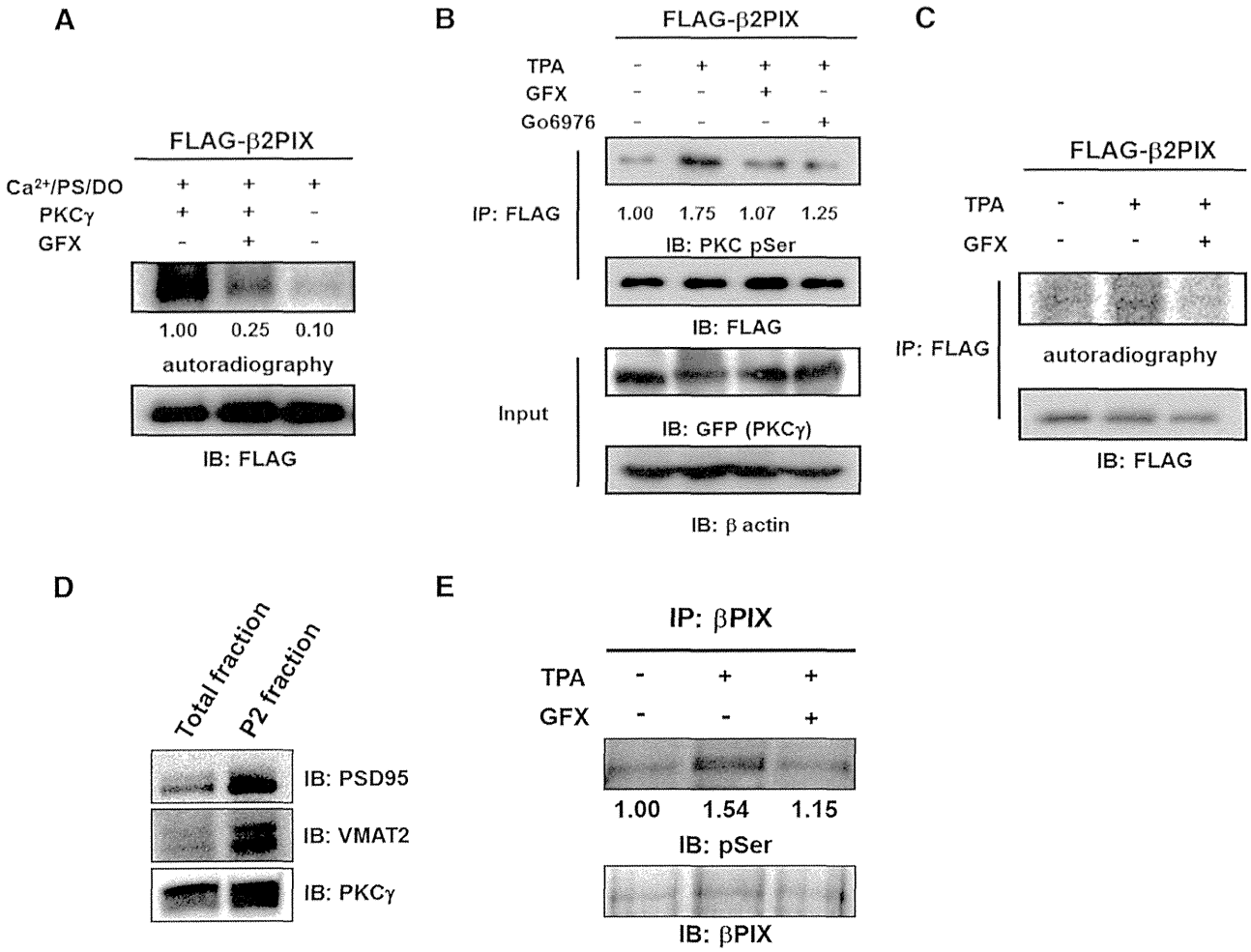

Figure 3. βPIX is phosphorylated by PKCγ *in vitro*, in cells, and *in vivo*. ***A***, *In vitro* phosphorylation of β2PIX. FLAG-tagged β2PIX proteins were purified and incubated with or without recombinant PKCγ in the presence of PKC activator (PS/DO/Ca^{2+}) and [γ-^{32}P] ATP for 20 min. The *in vitro* phosphorylation of β2PIX was also performed in the presence of GFX. The phosphorylated proteins were detected by autoradiography and the levels of protein expression were determined by Western blotting with an anti-FLAG antibody. The numbers show the relative phosphorylation levels that were normalized to PKCγ stimulation as 1.00 ($n = 3$). ***B***, In-cell phosphorylation of β2PIX. HEK293 cells expressing FLAG-tagged β2PIX and GFP-tagged PKCγ were stimulated with 1 μM 12-O-TPA for 20 min in the presence or absence of 1 μM GFX or 1 μM Gö6976. FLAG-tagged β2PIX proteins were purified with anti-FLAG agarose resin. Phosphorylated proteins were detected by an immunoblot analysis with an anti-pSer PKC motif antibody. Protein expression was determined by Western blotting with an anti-FLAG antibody. The average relative phosphorylation levels for each experimental condition were normalized to the prestimulation signal set as 1.00 ($n = 5$). ***C***, PC12 cells expressing FLAG-tagged β2PIX were incubated with ^{32}P monosodium phosphate and stimulated with 1 μM 12-O-TPA in the absence or presence of 1 μM GFX. FLAG-tagged β2PIX proteins were purified with anti-FLAG agarose resin. Phosphorylated proteins were detected by autoradiography, and protein expression was determined by immunoblots with an anti-FLAG antibody. ***D***, The same amount of samples of total fraction and the P2 synaptosomal fraction were immunoblotted by anti-PSD95 antibody as a postsynaptic marker, anti-VMAT2 antibody as a presynaptic marker, and anti-PKCγ antibody. ***E***, the P2 synaptosomal fraction was stimulated with 2 μM 12-O-TPA in the absence or presence of 2 μM GFX. βPIX proteins were purified with anti-βPIX antibody. Phosphorylated proteins were detected by phospho-Abs. The numbers show the relative phosphorylation levels that were normalized to pretreatment as 1.00 ($n = 3$).

DAT activity in PKCγ KO mice striatum. To evaluate the DAT activity in PKCγ KO mice, we performed the no-net-flux microdialysis experiment. The slope (extraction fraction) is the measure of the activity of DAT *in vivo*. Fig. 1*G* shows decreased DAT activity in the striatum of PKCγ KO mice, suggesting that PKCγ KO mice tend to have increased rather than decreased extracellular DA levels compared with WT mice (Fig. 1*F*). Consistent with our results, the increase in the serotonin release stimulated by high K^+ levels in WT was also significantly larger than that of the KO (Fig. 1*G*), as described previously in AS/AGU rats (Al-Fayez et al., 2005). Because we had preliminary data that suggested slight loss of DAergic neurons in 12-month-old, but not 3- or 6-month-old, PKCγ KO mice, there was a possibility that the decrease in DA release in PKCγ KO mice was due to the decrease in DA in the striatum. We measured DA and its metabolites using HPLC in the striatum. No difference in DA or DA metabolite levels in the striatum was observed between PKCγ KO mice and WT mice at 3, 6, and 12 months (Table 1), suggesting that DA release disorder was from the exocytotic machinery disorder instead of the lack of the DAergic neurons in the nigrostriatum system. These results suggested that the PKCγ KO mice would show similar parkinsonian symptoms as those observed in the AS/AGU rats. From the analysis of the PKCγ KO mice and AS/AGU rats, we concluded that PKCγ KO animals could be used as a practical model of parkinsonian syndrome.

Phosphoproteome analysis identified 10 phosphoproteins, including βPIX, with a PKC-phosphorylation motif

We hypothesized that a loss or decrease of PKCγ-mediated phosphorylation in the nigrostriatal system results in DA release im-

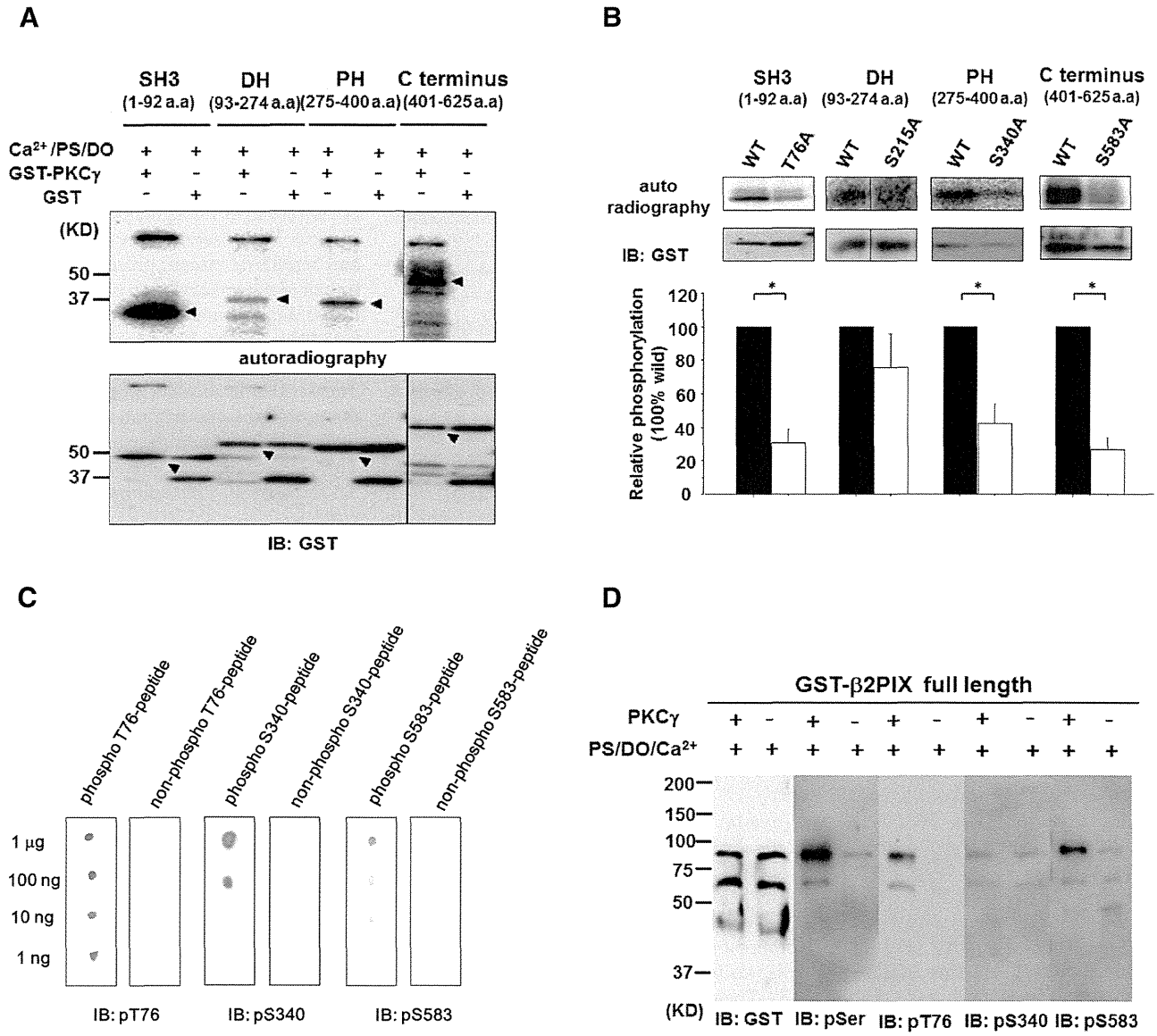

Figure 4. Analysis of the *in vitro* PKCγ phosphorylation sites in β2PIX. ***A***, *In vitro* phosphorylation of the GST-tagged β2PIX SH3, DH, PH, and C terminus regions. Each protein region was expressed in *E. coli*, purified, and incubated with [γ^{32}P] ATP and recombinant PKCγ in the presence of Ca^{2+}, PS, and DO. The phosphorylated proteins were separated by SDS-PAGE and detected by autoradiography (top). The protein levels of the recombinant β2PIX protein regions were detected by Western blotting (bottom). The arrowheads on the top indicate the autoradiography and those on the bottom indicate the total protein for each domain. ***B***, *In vitro* phosphorylation of the β2PIX SH3, DH, PH, and β2 C terminus regions containing the indicated mutations determined by an *in vitro* phosphorylation assay that was followed by mass spectrometry and phosphoproteome analysis. Phosphorylation levels were normalized to the WT phosphorylation signal for each domain, which were set to 100%: SH3 ($n = 5$), DH ($n = 4$), PH ($n = 5$), β2 C terminus ($n = 3$); The results are expressed as mean ± SEM (*$p < 0.05$, unpaired t test). ***C***, Specificity of anti-phospho-Thr76, Ser340, and Ser583 antibodies. The indicated amount of the phospho-peptide (pT76 [VSPKSG(pT)LKSPP], pS340 [SASPRM-(pS)GFIYQ], and pS583 [SLGRRS(pS)LSRLE]) or non-phosphopeptide was dotted on the PVDF membrane. Immunostaining was performed using purified anti-pT76, pS340, and pS583 antibodies. ***D***, *In vitro* phosphorylation assay of full-length β2PIX. GST-tagged full-length β2PIX was expressed in *E. coli*, purified, and incubated with ATP and recombinant PKCγ in the presence of Ca^{2+}, PS, and DO. Phosphorylated proteins were separated by SDS-PAGE and detected by an anti-pSer PKC motif antibody, an anti-pT76 antibody, an anti-pS340 antibody, or an anti-pS583 antibody, respectively.

pairment. To identify the substrates for PKCγ, we performed a phosphoproteome analysis using HAMMOC methods (Kyono et al., 2008; Fig. 2*A*). Among the phosphopeptides in the WT group, we chose the proteins that may have a relationship to exocytosis and then calculated the WT/KO ratio of the average ion intensity. The average ion intensity ratio of the phosphopeptides that included the PKC phosphorylation motif are shown in Table 2. Among these 10 candidates, we focused on βPIX (Fig. 2*B*), even when the degree of the phosphorylation decrease was small, because it is expressed in DAergic neurons in the SNpc (http://www.informatics.jax.org/assay/MGI:4944920) and has been reported to play important roles in the machinery of exocytosis (Audebert et al., 2004; Momboisse et al., 2009). In the present phosphoproteome analysis, phosphorylation of Ser340 in β2PIX was detected. The βPIX family consists of two splicing forms, β1 and β2; the difference between β1 and β2 PIX exists in the C terminus (Fig. 2*C*). Although both β1 and β2 contain Ser340, β2PIX is the predominant form in the CNS (Koh et al., 2001). Therefore, β2PIX was used in the present study.